Revision 1

Intermediate Members of the Lime-Monteponite Solid Solutions ($Ca_{1-x}Cd_xO$, x = 0.36-0.55): Discovery in Natural Occurrence

HANI N. KHOURY[1], ELLA V. SOKOL[2*], SVETLANA N. KOKH[2], YURII V. SERYOTKIN[2,3], OLGA A. KOZMENKO[2], SERGEY V. GORYAINOV[2], IAN D. CLARK[4]

[1]Department of Geology, The University of Jordan, Amman, Jordan 11942
[2]V.S. Sobolev Institute of Geology and Mineralogy, Siberian Branch of the Russian Academy of Sciences, 3 Koptyug Avenue, Novosibirsk, 630090 Russia
[3]Novosibirsk State University, Novosibirsk, 2 Pirogov Street, Novosibirsk, 630090 Russia
[4]Ottawa-Carleton Geoscience Centre, Department of Earth Sciences, University of Ottawa, 140 Louis Pasteur Street, Ottawa, Ontario, Canada K1N 6N5

*Corresponding author (sokol_ag@mail.ru; sokol@igm.nsc.ru)

ABSTRACT

Lime-monteponite solid solutions ((Ca,Cd)O ss) with 58.5-73.3 wt% CdO were discovered as an accessory phase in medium-temperature combustion metamorphic (CM) spurrite-fluorellestadite/ fluorapatite marbles from central Jordan. The type locality is situated in the northern part of the Siwaqa complex (Tulul Al Hammam area), the largest area of the "Mottled Zone" Formation in the Dead Sea region. The marbles were derived from bitumen-rich calcareous marine sediments of the Muwaqqar Chalk Marl Formation which have high Cd, Zn, U, and Ni enrichments and contain Cd-rich wurtzite and sphalerite. Oxidative sintering of these sediments at 800-850 °C gave rise to unusual oxide accessories: lime-monteponite solid solutions, Cd-bearing Ca and Zn aluminate – tululite, zincite, and Zn-, Ni- and Cu-rich periclase. Cadmium incorporation into different oxides was controlled by steric factors, while $Cd^{[6]} \rightarrow Ca^{[6]}$ was the principal isomorphic substitution. The intermediate members $(Ca_{0.645}Cd_{0.355})O$ – $(Ca_{0.453}Cd_{0.547})O$ with a halite-type structure have a cadmium incorporation ratio ($K_{Cd} = Cd_{mineral}/Cd_{rock}$) of about 843 and are the main sites for cadmium in CM marbles. In supergene environments, at low water/rock ratios, $(Ca_{1-x}Cd_x)(OH)_{2\ ss}$ ($x \leq 0.5$) constitute the main secondary phase after (Ca,Cd)O ss. At higher water/rock ratios and in the presence of Cl^- and F^- in the solutions, calcium and cadmium precipitated as separate phases (fluorite (CaF_2) and basic

cadmium chloride ($Cd(OH)_{2-x}Cl_x$)). A part of cadmium becomes retained in calcium silicate hydrates. The common occurrence of anhydrous (Ca,Cd)O grains in natural rocks, only partly altered to (Ca,Cd)-hydroxide after at least 100 ka exposure to weather and climate, proves that both phases are effective long-term Cd immobilizers.

Key-words: lime-monteponite CaO-CdO solid solution, cadmium enrichment, hydrous alteration, combustion metamorphism, central Jordan

INTRODUCTION

The upper crustal abundances of Cd and Zn are 0.09 ppm and 67 ppm, respectively, and the Cd/Zn ratio is 0.001 (Rudnick and Gao 2003). Since cadmium is similar to zinc in its crystal-chemistry and geochemical behavior, it is hosted chiefly by sphalerite and fails to form commercially viable deposits (Ye and Liu 1999; Schwartz 2000; Ye et al. 2012). Worldwide, the average cadmium to zinc ratio is about 1/400 in zinc ores. The mean contents of Cd in sphalerites range between 0.2 and 0.6 wt% (Ye and Liu 1999; Schwartz 2000). Cadmium content is much higher in sedimentary-exhalative (SedEx) and Besshi-type volcanic massive sulfide deposits (up to 1.0-2.5 wt% Cd in sphalerite). The highest cadmium concentrations up to 5 wt%, with an average of 1.4 wt% Cd are reported in sphalerite from the carbonate-hosted Mississippi Valley-type (MVT) Zn-Pb deposits, where the low S^{2-} activity favored the formation of Cd-rich sphalerite (Schwartz 2000; Ye et al. 2012).

Besides sphalerite, Cd has been occasionally found as impurity in tetrahedrite (Pattrick and Hall 1983; Dobbe 1992), freibergite (Pattrick 1978) or the metacinnabar-variety saukovite (Hg,Cd)S, considered an intermediate member of the metacinnabar-hawleyite series (Fleischer 1966). The few known cadmium minerals (27 mineral species) are: sulfides and sulfosalts (11), phosphates and arsenates (6), sulfates and selenates (7), carbonates (1), oxides (1) and native elements (1). The relatively common minerals are greenockite (CdS, hexagonal) and otavite ($Cd(CO_3)$). Cadmium minerals (greenockite, otavite, monteponite (CdO), cadmoselite (CdSe), hawleyite (CdS, cubic), native cadmium, and niedermayrite ($(CdCu_4(SO_4)_2(OH)_6 \cdot 4H_2O)$) occur in the zone of chemically weathered sulfide zinc ores. Their presence can be attributed to Zn scavenging by secondary smithsonite ($ZnCO_3$) and/or hemimorphite ($Zn_4(Si_2O_7)(OH)_2 \cdot H_2O$) crystallization (Ye and Liu 1999; Schwartz 2000; Ye et al. 2012).

The unusual mineral of a $Ca_{1-x}Cd_xO$ ($x = 0.36$-0.55) composition discussed in this paper belongs to the lime-monteponite solid solution series and comes from particular calcareous combustion metamorphic (CM) rocks of Jordan (the so-called Mottled Zone, Levant, Dead Sea area). It was identified for the first time by the first author during screening of a voluminous collection of CM

marbles from central Jordan (Khoury et al. 2014b). Later detailed field and SEM examination of phosphate-rich marbles, which have been found at a local site within the Tulul Al Hammam area, showed that (Ca,Cd)O was an indicative accessory mineral of the marbles formed under oxidative sintering of Cd-containing, phosphate- and bitumen-rich chalky protolith.

The following work aims to characterize comprehensively the intermediate members of the lime-monteponite solid solution series, to estimate cadmium and zinc incorporation into different phases and crystal structures in Ordinary Portland Cement (OPC) clinker-like medium-temperature assemblages, and to identify the secondary Cd-bearing compounds that formed and survived during long acting supergene alteration of the marbles.

GEOLOGICAL BACKGROUND

Unusual Cd mineralization together with various Ca-U(VI) oxides were identified in the combustion metamorphic rocks, known under a local name of *varicolored marbles,* central Jordan (Daba-Siwaqa complex of the Mottled Zone) (Khoury et al. 2015). For details of local geology see (Khoury et al. 2014a, 2015). The rocks were derived from marine sediments, exposed everywhere in central Jordan, which were deposited at shallow depths in a stable shelf high-productive environment from the Late Cretaceous to the Early Eocene (ca. 90 – 50 Ma ago) and belong to the Belqa Group (Ziegler 2001; Abed et al. 2005; Powell and Moh'd 2011; Fleurance et al. 2013; Khoury et al. 2015). Their gentle folding and faulting were mostly related to the continued tectonic movement along the Dead Sea-Jordanian Transform located ~60 km to the west of the Daba-Siwaqa area (Bender 1968, Powell and Moh'd 2011). Two fault sets dominate in the Daba area: an E-W extension of the Zarqa-Ma'in fault and the NW-SE striking Wadi Al Hammam fault set. The organic-rich sediments were uplifted during the Quaternary time, exposed at the surface, and subjected to spontaneous oxidation and *in situ* combustion of the hosted bitumen and disseminated sulfides within the tectonically disturbed zones (Techer et al. 2006; Khoury et al. 2011). In Jordan the CM rocks, mostly marbles, cover large areas in the Daba, Siwaqa, Khushaym Matruk, Suweilih, and Maqarin complexes (Figs. 1, 2) (Khoury and Nassir 1982 a,b; Techer et al. 2006; Fourcade et al. 2007; Elie et al. 2007; Khoury 2012; Fleurance et al. 2013).

The type locality of the (Ca,Cd)O phase is called Tulul Al Hammam *(*Arabic for *Pigeon's Hill*), (31°32′N 36°12′E), and is situated in the northern Siwaqa area (Khoury et al. 2014a, 2015; Khoury and Al-Zoubi 2014) (Fig. 1). Varicolored CM marbles typically occur as lenticular bodies from a few meters to more than 60 m thick and form cliffs and hills. The hills are arranged in sub-parallel belts (0.2-3 km wide and 1-10 km long) related to faults of the Daba system (Fig. 1). The marbles are derived from the Maastrichtian-Paleogene Muwaqqar chalk and marl enriched in phosphorous, organic

matter, and trace elements, including Cd, Zn, and U (Table 1). The whole sequence crops out along the valleys (*wadis*), where bituminous chalk and marl are overlain by CM rocks, unconformable Pleistocene travertine, fluvial to lacustrine deposits, and Holocene to Present alluvium.

The CM marbles vary in color from black and brown to red, pink and green, depending on their mineralogical composition, and the degree of alteration (Figs. 2a-c). The color diversity appears at all levels, from outcrop to hand specimen (Khoury et al. 2015). In many outcrops, marbles are rather fresh and preserve the original lamination of precursor sediments. Fresh marbles rich in disseminated sulfides are black, while the altered varieties, as well as those enriched in fresh Ca-ferrites, are brown; strongly altered marbles are pale red or pink. Green marbles are rich in fluorapatite and/or fluorellestadite and have bluish tints specific to CM ellestadites (Zateeva et al. 2007; Kokh et al. 2015). Fresh massive samples often show thin bands up to 3cm of alternative colors that reflect uneven distribution of sulfides and phosphates in the parent rocks.

MATERIALS AND METHODS

(Ca,Cd)O mineral grains were identified in seven samples, after initial scrutiny of about sixty marble samples from the Tulul Al Hammam quarries. In the beginning of the project, several tens of Cd-bearing grains, including micrometer particles, were characterized by quick scanning and imaging at the Department of Earth Sciences, University of Ottawa. Five selected samples of marbles bearing Ca-Cd oxide (TH-11, TH-18, TH-72, TH-74, DT-7) and typical sedimentary parent rock (Daba oil shale, DOS-1) were then studied by optical thin section petrography, with SEM, EPMA and Raman spectroscopy for additional details at the V.S. Sobolev, Institute of Geology and Mineralogy (IGM, Novosibirsk, Russia).

The bulk compositions of major and trace elements were analyzed by atomic emission-spectrometry with inductively-coupled plasma (ICP-AES) (IRIS Advantage ThermoJarrell, Intertechs Corporation, USA) at IGM. The powdered sample was mixed with lithium metaborate, and then fused at 1050ºC. Sample concentrations were measured after dissolution in 5% nitric acid (Shatsky et al. 2006). The analytical precision was about 10-15 %. Trace-elements (Th, U, and Y) were analyzed at the Siberian Synchrotron and Terahertz Radiation Centre (SSTRC) at Budker Institute of Nuclear Physics, Novosibirsk, using precise synchrotron radiation X-ray fluorescence analyses (SR XRF) with EDS (energy-dispersion spectroscopy), at 23 kV and 42 kV excitation energy (Phedorin et al. 2000).

Organic fractions (TOC) were extracted from the sedimentary protolith sample following the procedure from (Selby and Creaser 2003). C-H-N-S analyses of TOC were carried out at the N.N. Vorozhtsov Novosibirsk Institute of Organic Chemistry SB RAS (NIOCH SB RAS,

Novosibirsk), according to (Fadeeva et al. 2008) using *Hewlett-Packard*, *model 185* (United States) and *Euro EA 3000* (Italy) analyzers.

Thin sections of the marbles and sediments were prepared using standard equipment and protocol (e.g., Humphries 1992). Polished thin (20–30 μm) sections in epoxy resin were used for optical studies. The thin-section top surface was polished and the sections were studied with both transmitted and reflected light. Petroleum was used for coolant/lubricant to accommodate preparation of hydrophobic materials. Thin sections were finished by polishing using 0.25 μm diamond paste. Prior to assessment in SEM, polished sections were sputter coated with ~30 nm gold (Au), for chemical analysis using EPMA as well as for elemental mapping using SEM with carbon (C).

First Cd-bearing phases were characterized on a *A JEOL JSM 6610LV* electron microscope (SEM) equipped with an Oxford INCA large area SDD detector (for qualitative analysis of Be to U elements) at the University of Ottawa. Then the microfabric and phase distribution of the samples were assessed on a JEOL JSM6380LA scanning electron microscope (at IGM) on both Au- and C-coated polished thin sections, at chamber vacuum pressure 10–5 Torr (~0.01 Pa). The instrument was operated at 10 kV and 2.0 nA beam current (Faraday cup). The images were acquired in both SE and BE modes. SEM and EDS techniques were applied to grains smaller than 1-5 μm to determine their morphology, mineral chemistry, compositional variations, and the alteration degree of Ca-Cd oxides.

Quantitative mineral analyses were performed using a *JEOL JXA 8230* Super Probe (EPMA). The X-ray diffraction data were collected on a *Philips* powder X-Ray diffractometer with a double goniometer *X'Pert* system (CuKα-radiation with $\lambda = 1.54178$ Å) at the University of Ottawa.

Afterwards, chemical compositions of individual minerals were analyzed at IGM using a *JEOL JXA 8100* microprobe, in C-coated polished thin sections, with chamber vacuum kept at 10^{-6} Torr (~0.001 Pa) or better. The EPMA measurements were conducted with an accelerating voltage of 20 kV, the peak count time was 10 s, the beam current was 20 nA, and the beam diameter was 2–3 μm for anhydrous minerals. Volatile-rich phases were analyzed at an accelerating voltage of 20 kV, a lower beam current (10 nA) and a shorter peak count time (5 s) in order to minimize damage from the beam. Measurement of F was allocated to a WDS-TAP detector at the start of an analytical run, to further minimize evaporation artifacts (Morgan and London 2005). Only the particles larger than 5 μm were taken into consideration to avoid errors caused by the matrix capture. The compositions were estimated with reference to natural and synthetic standards: diopside (Ca), pyrope O-145 (Si, Al, Fe, Mg), CdS (Cd, S), $ZnFe_2O_4$ (Zn in oxides) or ZnS (Zn in sulfides), Sr-Si glass Gl-11 (Sr), TiO_2 (Ti), fluorapatite (P, F), chlorapatite (Cl). Matrix correction using the PAP routine was applied to raw data prior to recalculation into major oxides. The analytical accuracy was better than 2 %-relative to >5 wt% elements and about 5 %-relative to ≤ 2 wt% elements and F. For detection limits of elements

see Table 3. Oxide contents are recalculated into atoms per formula unit (apfu) following routine procedures (e.g., according to Deer et al. (1992) or Papike (1987, 1988)).

Single-crystal X-ray study of a $Ca_{0.5}Cd_{0.5}O$ grain was carried out using an *Oxford Diffraction Xcalibur Gemini* diffractometer, Mo*K*α, λ = 0.71073 Å (Novosibirsk State University, Novosibirsk). Diffraction data were collected by scanning of ω angle with step of 1º per frame (ω scan technique). The data were processed using *CrysAlis Pro* (Oxford Diffraction 2008). Semi-empirical absorption correction was applied using the multi-scan technique.

Raman spectra were recorded on a *Horiba Jobin Yvon LabRAM HR800* spectrometer with a 1024 pixel LN/CCD detector using the 514.5-nm emission line of Ar^+ ion laser with the 50 mW maximum beam power (up to 17 mW on the sample surface). The spectra were collected in a back-scattering geometry, using an *Olympus BX41* microscope (Goryainov et al. 2012, 2014). The spectral resolution of the recorded spectrum Stokes side was set to ~2.2 cm^{-1} at a Raman shift of ~3000 cm^{-1}. This resolution was achieved by using one grating with 1800 grooves/mm and equal 150 µm slit and pin hole sizes. The microscope with an *Olympus PlanLWD 50X* objective lens of a working distance WD = 11 mm with 0.5 numerical aperture provides a focal spot diameter of ~ 2 µm on the sample surface. The Raman spectra were deconvolved into Voigt amplitude functions using the *PeakFit* software (Model S506 Interactive Peak Fit, 2002).

SEDIMENTARY PARENT ROCKS: LITHOLOGY, MINERALOGY, GEOCHEMISTRY

The Belqa Group sedimentary sequence encloses large economic-scale beds of phosphorites buried under bituminous chalk and marl, with C_{org} up to 25 wt% and disseminated francolite. The sediments are remarkable by very high relative enrichments in Cd, Cr, Mo, Ni, U, V, Zn, and Se (Abed et al. 2005; Abed 2012; Abed and Sadaqah 2013; Fleurance et al. 2013). They have relatively high contents of both P and Cd but low Co (< 3-12 ppm) and Mn (< 0.01 wt%), which is typical of sediments from the upwelling zone (Nathan et al. 1997; Delgadillo-Hinojosa et al. 2001; Brumsack 2006).

The CM marbles exposed at the Tulul Al Hammam area are derived from bituminous chalk and marl (locally known as 'oil shales') of the lower Muwaqqar Chalk Marl Fm. at the top of the Belqa Group (Abed et al. 2005; Powell and Moh'd 2011; Fleurance et al. 2013; Khoury et al. 2015). We analyzed a typical sample (DOS-1) of non-metamorphic chalky protolith from a site in the Daba area. The fine-grained gray bituminous chalk is laminated, and contains abundant shell clasts and planktonic foraminifera (*Globigerinoides, Anomalinoides, Cibicides, Turrilines, Subbotine*; Figs. 3d and e). The rock consists mainly of calcite and a minor amount of fine clayey matter. Biogenic carbonate-fluorapatite (francolite) occurs as skeleton fragments and irregular nodules, some being oriented along

the lamination. The sediment encloses porous clots of radiolarian spicules (consisting of cristobalite opaline matter) and has 22.8 wt% C_{org}. Bitumen matter from this sediment stores 40 wt% C, 4.8 wt% H, 1.3 wt% N, and 7.8 wt% S; organic matter filling the shells (Fig. 3e) contains up to 9 wt% sulfur on average.

The sample DOS-1 bears high contents of Cd (224 ppm) and Zn (1498 ppm) and abundant sulfides (Table 1 and Fig. 3). The chalk matrix contains disseminated framboidal pyrite with V and Ni impurities (both ~ 0.4 wt%) (Fig. 3a). Cd-rich wurtzite is the main sulfide mineral sometimes coexisting with Cd-rich sphalerite. Both minerals occur most often in free space of shells as intergrowths of rather large and perfect crystals (Figs. 3b-d and f). Many micrometer-sized platy crystals of (Zn,Cd)S form tight aggregates with radiolarian spicules (Fig. 3b) while coarser and more perfect platy wurtzites and tetrahedral or pseudo-octahedral twin sphalerites in the matrix most likely result from re-crystallization of finer imperfect (Zn,Cd)S grains (Figs. 3c and f). The average wurtzite composition is 55.88 (55.5-56.6) wt% Zn, 8.91 (8.0-9.6) wt% Cd, and 31.25 (31.3-32.6) wt% S, with the impurities of 0.74 wt% Cu (on average), 0.44 wt% Fe, and 0.52 wt% As. The average chemical composition of sphalerite is 56.64 (56.3-57.0) wt% Zn, 8.29 (7.7-9.2) wt% Cd, and 32.49 (32.2-32.9) wt% S, 0.54 wt% Cu, 0.30 wt% Fe, and 0.28 wt% As. The average compositions of the two minerals correspond to $(Zn_{0.88}Cd_{0.08}Fe_{0.01}Cu_{0.01})_{\Sigma=0.99}S_{1.01}As_{0.01}$ and $(Zn_{0.88}Cd_{0.07}Fe_{0.01}Cu_{0.01})_{\Sigma=0.97}S_{1.03}$, respectively. Thus a representative sample of bituminous chalk from the Muwaqqar Chalk-Marl Formation as the non-metamorphic precursor of CM marble contains abundant Cd-rich wurtzite and sphalerite (Cd/Zn ~ 0.15).

COMBUSTION METAMORPHIC MARBLE: MINERAL CONTENT AND COMPOSITION

Intermediate members of the CaO-CdO $_{ss}$ were found as accessory minerals in the fine-grained spurrite-fluorellestadite/fluorapatite marbles, typical medium-temperature (T ~ 800-850˚C) CM rocks formed by partial decarbonation and sintering of calcareous bitumen-rich chalks (Khoury et al. 2014b, 2015). The marbles are varicolored homogeneous (or rarely foliated), massive, and microcrystalline (up to 50 μm). They consist of 80-90 vol% calcite, and 2-15 vol% fluorapatite or fluorellestadite ($Ca_5(SiO_4)(PO_4)(SO_4)F$) segregated into thin layers, as well as ≤5 vol% Na-and P-bearing spurrite ($Ca_5(SiO_4)_2(CO_3)$), Ti-, Cr- and/or Zn-bearing brownmillerite ($Ca_2(Fe_{1-x}Al_x)_2O_5$), and sporadic micrometer-sized grains of partially hydrated or hydroxylated fluormayenite ($Ca_{12}Al_{14}O_{32}F_2$) and/or chlormayenite ($Ca_{12}Al_{14}O_{32}Cl_2$) (Table 2, Figs. 4 – 6). Samples TH-18 and TH-72 also contain high fluorine Ca aluminate (< 1 to 10 μm in size) with 52.22-53.51 wt% CaO, 32.06-34.03 wt% Al_2O_3, 0.64-0.98 wt% SiO_2, 0.77-1.84 wt% Fe_2O_3, and 5.00-5.81 wt% F. All compositions are total deficient (90-92 wt%), i.e., the mineral likely underwent hydration.

The majority of the marbles in the area ((dark and black varieties (Fig. 2a)) are rich in disseminated sulfides indicating their origin under reducing conditions at a greater availability of fuel (dispersed bitumen matter and primary sulfides) relative to the oxidizer (atmospheric oxygen), i.e., at high fuel/oxidizer ratios. Yellow sphalerite, the most abundant CM sulfide, contains 0.8-1.7 wt% Cd, 1.0-2.1 wt% Fe, and 0.4 – 1 wt% Se. Fine grains of greenockite (CdS), acanthite or argentite (Ag_2S), samaniite ($Cu_2Fe_5Ni_2S_8$), and Cu-rich djerfisherite ($K_6Na(Cu,Fe,Ni)_{25}S_{26}Cl$) are common phases, whereas pyrrhotite, galena, chalcopyrite, and oldhamite (CaS) are found very rarely as single fine particles.

Numerous large grains of intermediate members of the CaO-CdO solid-solution series were detected in three marble samples (DT-7, TH-72, TH-18) containing 3.44-7.20 wt% P_2O_5 and 100-697 ppm Cd (Table 1, Figs. 2c and 4-6). These Cd concentrations are commensurate with the average values in the marbles (~130 ppm according to Fleurance et al. (2013)) and in their sedimentary precursors (197 ppm after Fleurance et al. (2013)). The marbles with lower Cd contents (28-75 ppm) (TH-11, TH-74) only contain sporadic, finely dispersed grains of intermediate lime-monteponite series minerals up to 5μm. The presence of rock-forming fluorellestadite and/or sulfate-bearing fluorapatite in marbles (TH-11, TH-18, TH-72, DT-7 in Table 2) implies oxidative sintering during combustion metamorphism (Parat et al. 2002; Zateeva et al. 2007; Marks et al. 2012; Kokh et al. 2015).

Other important Cd-bearing accessories are Ca and Zn aluminate, tululite ($(Ca,Cd)_{14}(Fe^{3+},Al)(Al,Zn,Fe^{3+},Si,P,Mn,Mg)_{15}O_{36}$) with 5-8.5 wt% of CdO, just approved as a new mineral (Figs. 4a and 5) (Khoury et al. 2014c), and zincite with 0.8-3 wt% of CdO. Brownmillerite, the main opaque mineral of the marbles, includes 1-3.5 wt% of ZnO, but is free from Cd. Zn-rich periclase (ZnO – 20-24 wt%; NiO – 5-6 wt%; CuO – 2.6-3.3 wt%) is also free from Cd (Table 2; Figs. 5 and 6f). Other oxide accessories are Ca uranates ($CaUO_4$, Ca_2UO_5, Ca_3UO_6) (Figs. 6a and c), cuprite (Cu_2O) (Fig. 4d), tenorite (CuO), cassiterite, Th-bearing cerianite $(Ce,Th)O_2$, U-bearing lakargiite ($Ca(Zr,Ti,U)O_3$), most of them found as individual micrometer-sized grains (< 1 to 10 μm).

The TH-11 marble is an unusual sample, where Cd-bearing sphalerite (with 0.8-1.2 wt% of Cd), galena, and silver minerals such as Ag^0, Ag_2S, iodargirite (AgI) are superposed with zincite, sporadic fine grains of (Ca,Cd)O, bunsenite (NiO), and lime (CaO) (Table 2). Oxide and sulfide accessories occur in different micro-layers of the former sediment.

The marbles are unevenly hydrated and altered (Fig. 2b and Table 2). Fluorapatite, fluorellestadite, and brownmillerite commonly remain intact. Spurrite is frequently replaced by calcium silicate hydrates (CSHs). Both fluormayenite and chlormayenite, having high hydraulic reactivity (Taylor, 1997; Galuskin et al., 2015), are partially hydrated or hydroxylated. The main alteration products are secondary Ca-carbonates, namely aragonite, CSHs, hydrogarnets, including Cl-

bearing varieties, and hydrated phases after Ca aluminates (fluormayenite, chlormayenite, and high fluorine Ca aluminate).

(Ca,Cd)O solid solutions

The finest grains ≤ 5 μm of intermediate lime-monteponite (Ca,Cd)O minerals are anhedral and typically hosted by calcite and spurrite, or more rarely by fluorellestadite; they occur in phosphate-rich thin layers associated with Ca-U(VI) oxides. Coarser grains 15-20 μm are anhedral to subhedral showing {100} and {111} faces (Figs. 4 and 6). The coarsest grains ~70 μm have an irregular habit, may be partially hydrated along edges, and commonly contain inclusions of fluorellestadite/fluorapatite, brownmillerite, spurrite, calcite, or rarely Zn-rich periclase. All (Ca,Cd)O grains examined here are monocrystalline and appear contiguous in SEM without discernible internal boundaries. No randomly intergrown polycrystalline or twinned grains common to monteponite have been identified in the intermediate lime-monteponite series members we studied.

The mineral is pale yellowish-green with vitreous lustre, very brittle and transparent. It is optically isotropic but some grains show local anisotropy, probably due to internal strain. The cleavage is distinct on {111} (Fig. 6b). The Mohs hardness is (3-3½), as measured by microindentation (VHN load 5 g, mean of 10 = 140 kg/mm^2). Density could not be measured because of small grain sizes. The calculated density is 5.703 g/cm^3 (based on the empirical formula). The mineral dissolves in 0.1 % HCl.

Mineral chemistry

The chemistry of intermediate members of the lime-monteponite solid-solution series (Table 3) was analyzed in a few tens of grains using a microprobe with an EDS analyzer at the University Ottawa and at the Institute of Geology and Mineralogy (Novosibirsk). The compositional variation of (Ca,Cd)O solid solutions is minimal within each sample (Fig. 7a). The examined fresh grains are homogeneous and lack any zoning for the elements shown. The CdO content varies between 58.54 wt% (TH-18) and 73.25 wt% (DT-7), and the corresponding CaO concentrations are 41.46 wt% and 26.51 wt%, respectively. ZnO (< 0.2-0.93 wt%) is the only significant impurity, while other impurities (Al, Fe, Mg, Ti, and Sr) are negligible. Thus the composition range of the natural CM lime-monteponite ss is: $(Ca_{0.645}Cd_{0.355})O$ – $(Ca_{0.453}Cd_{0.547})O$ (Fig. 7b).

X-ray data and crystal structure

Crystal structure was determined in a (Ca,Cd)O grain (~50×40×30 μm) extracted from sample DT-7, along the edges altered to $CaCd(OH)_4$ (Fig. 6d). The mineral $(Ca_{0.49}Cd_{0.51})O$ is cubic,

$a = 4.75377(14)$ Å, $V = 107.427(6)$ Å^3, $Z = 4$. The unit-cell size was refined on the basis of 497 reflections (Table 4). The systematic absence of reflections is consistent with the space-group $Fm\bar{3}m$. The solution and refinement of the crystal structure on the basis of F^2 was made using the SHELX program package (Sheldrick 2008). Like the pure series endmember lime (CaO) and monteponite (CdO), the natural intermediate $(Ca_{0.49}Cd_{0.51})O$ has a NaCl-type structure, without any discernible ordering of Ca and Cd. The unit-cell *a*-parameter of $(Ca_{0.49}Cd_{0.51})O$ corresponds to the average of CaO (Fiquet et al. 1999) and CdO (Zhang 1999) metrics.

For $(Ca_{0.49}Cd_{0.51})O$, we calculated the valence of cations using the bond valence sum (BVS) formula in which each bond with a distance d_{ij} contributes the valence $v_{ij} = \exp[(R_{ij} - d_{ij})/0.37]$ with R_{ij} as an empirical parameter, and the total valences of atom i, V_i equals $V_i = \sum_j v_{ij}$ (Brese and O'Keeffe 1991). The calculated valences of cations are +1.82, +1.81, and +1.83 for the CaO, CdO, and $(Ca_{0.49}Cd_{0.51})O$ structures, respectively.

RAMAN SPECTROSCOPY

The Raman spectra were recorded for a large grain (~ 70 µm) with a $Ca_{0.51}Cd_{0.49}O$ core and a thick $CaCd(OH)_4$ rim (Table 5, sample DT-7). The (Ca,Cd)O phase, with its cubic unit cell ($Fm\bar{3}m$), lacks the first order Raman scattering, like other compounds with the NaCl structure (Rieder et al. 1973; Smyth et al. 2000; Murtaza et al. 2012). The $Ca_{0.51}Cd_{0.49}O$ phase shows second-order scattering (Fig. 9a). The most intense bands have been interpreted according to (Rieder et al. 1973) as 2TA(X) 501 cm^{-1}, TA+TO(X) 611 cm^{-1}, 2TO(X) 704 cm^{-1}, and 2LO(L) 1079 cm^{-1}. A weak 3582 cm^{-1} band in the domain of O-H stretching vibrations is due to $CaCd(OH)_4$ hydroxide.

Mixed Ca-Cd hydroxide $CaCd(OH)_4$, being isostructural with $Ca(OH)_2$ and $Cd(OH)_2$ crystals in the CdI_2-type structure $P\bar{3}m1$, Z = 1, at ambient conditions, has total irreducible representation at the Brillouin zone centre: $\Gamma = 2A_{1g} + 3A_{2u} + 2E_g + 3E_u$ (Shieh and Duffy 2002). Four modes are active in the first order Raman scattering $2A_{1g} + 2E_g$, of which three are lattice modes and one is symmetric A_{1g} O-H stretching vibration. Three Raman modes of $CaCd(OH)_4$ are reliably identified in the spectrum of Fig. 9b: E_g 216 cm^{-1}, A_{1g} 367 cm^{-1} and A_{1g} 3589 cm^{-1}, the second and third bands being the most intensive. The bands of calcite admixture are labelled 'Cal' in Fig. 9a.

PRODUCTS OF (CA,CD)O ALTERATION

Grains of (Ca,Cd)O larger than 10-15 µm in diameter commonly have altered rims (Figs. 4c,d; 6d and 10; Table 5). In the freshest and densest marble DT-7 the hydrated rims vary in width from 0.1 to 0.5 grain diameter of the anhydrous precursor (Figs. 4d and 6d). The substitution front is directed inward

from the (Ca,Cd)O grains boundary while there is no signature of Cd leakage outside its limits. The hydrated compound contains 25.4 wt% CaO and 56.8 wt% CdO (on average), with impurities of SiO_2 (0.41-1.45) and Cl (0.27-0.53) (Table 5), that corresponds with the chemical formula $CaCd(OH)_4$. The newly-identified naturally-occurring phase $CaCd(OH)_4$ is discovered for the first time and has been confirmed by X-ray diffraction (Fig. 8) and Raman spectroscopy (Fig. 9b). The position of Debye arcs in 2D frames conform ICDD card file 00-050-0246 for synthetic $CaCd(OH)_4$ (Fig. 8). Furthermore, sample DT-7 contains spurrite and chlormayenite hydrated along the edges, and anhydrous Ca-U(VI) oxides partly replaced by Si-bearing $CaO\text{-}UO_3$ compounds (Tables 2 and 5). Alteration is most significant in sample TH-72, which bears calcium silicate hydrates (CSHs), hydrogarnets, and brucite, besides halite and fluorite.

The most obvious redistribution of Cd, marked by a train of its leakage from $(Ca,Cd)O_{ss}$ grains, was observed in the TH-72 marble sample containing quite strongly hydrated spurrite, fluormayenite, and periclase (Table 5). The coexisting grains of altered $(Ca,Cd)O_{ss}$ and fluorite have thin (2-5 μm) rims containing 56-79 wt% Cd, 5-11 wt% Ca, 12.6-20.0 wt% O, and 9-11 wt% Cl determined by EDS, as well as 1.8-8.7 wt% F at some sites (Table 5). Furthermore, Cd- and Cl-bearing compounds occur in cracks and impregnate the mechanically soft aggregates of Ca hydrosilicates with porous fabric. Such mineral aggregates with high Cd (53-69 wt% CdO) enrichment and variable contents of CaO (7.2-14.7 wt%), Cl (5.2-7.2 wt%), and F (2.2-6.3 wt%) were found on fresh cracks near altered (Ca,Cd)O grains.

Note that tululite (Khoury et al. 2014c) with 5-8.5 wt% of CdO, second strongest immobilizer of Cd, which coexists with (Ca,Cd)O grains in both samples (DT-7 and TH-72), bears no traces of dissolution, substitution or hydration (Fig. 5).

DISCUSSION

Monteponite and lime: natural occurrences

The geochemical cycle of cadmium follows closely that of zinc. In the hydrothermal environment, the Cd/Zn ratio is generally not high enough to allow crystallization of independent cadmium minerals (especially, CdS greenockite or hawleyite). Sphalerite is the chief host of cadmium in zinc deposits. Cadmium may be readily separated from Zn and become mobilized in the oxidation zone during post-depositional alteration of Cd-rich sulfide ores, which gives rise to smithsonite-hemimorphite ± zincite, hydrozincite Zn mineralization and monteponite ± otavite Cd mineralization (De Waele et al. 1999; Schwartz 2000; Ye et al. 2012).

Monteponite (CdO) was named after Monteponi, its type locality in Sardinia, where the mineral was found for the first time in the oxide zone of secondary non-sulfide Zn ores, mainly smithsonite ($Zn(CO_3)$) and hemimorphite ($Zn_4(Si_2O_7)(OH)_2 \cdot H_2O$). The primary Cd-rich sulfide ores belong to the MVT deposits. The Sardinian monteponite exists as perfect crystals inside terra rossa sediments deposited in natural paleokarst pockets and coexists with zincite, cuprite, baryte, smithsonite, melanterite ($Fe(SO_4) \cdot 7H_2O$), and hydrozincite ($Zn_5(CO_3)_2(OH)_6$) (Forti 1985; Forti and Perna 1988; De Waele et al. 1999; De Waele and Forti 2005).

Another example was reported from the oxide zone of the MVT Niujiaotang Cd-rich zinc deposit among Early Cambrian carbonate rocks (Guizhou province, SW China). Primary sphalerite is enriched in cadmium (average 1.4 wt% Cd). Greenockite, otavite, and cadmium oxides formed as secondary phases during chemical weathering (leaching) of sulfide ores, along with the formation of limonite, smithsonite, and hemimorphite (Ye and Liu 1999; Ye et al. 2012).

Monteponite was also found together with Cd sulfides and sulfosalts precipitated from high-temperature (T=400-910˚C) gases in the fumarolic fields of Kudriavy Volcano in Iturup Island, the Kuriles (Russia). It may result from oxidation of primary Cd-rich sulfides of the system ZnS-CdS (2.4-69.5 wt% of Cd), while gas-transport reactions contribute to the deposition of mineral rarities such as cadmoindite ($CdIn_2S_4$), kudriavite $(Cd,Pb)Bi_2S_4$ (Chaplygin et al. 2004, 2005, 2007) and pure rhenium mineralization (Korzhinsky et al. 2004**)**.

The occurrence of lime is restricted to high-temperature pyrometamorphic and/or combustion metamorphic calc-silicate assemblages produced by the melting-free decarbonation reaction $CaCO_3 \rightarrow CaO + CO_2\uparrow$ between 900 and 1250 °C at 1 and 40 bar P_{CO_2}, respectively (Bowen 1940; Tilley 1951; Treiman and Essen 1983; Grapes 2011). Natural examples of this reaction were recorded in limestone xenoliths in tephritic lava from the Eifel (Germany) and Vesuvius (Zambonini 1936), sites where lime was found (Grapes 2011).

Lime, with its extremely high hydraulic reactivity, reacts quickly with water or water vapor to form highly soluble and reactive portlandite ($Ca(OH)_2$) (Taylor 1997). Therefore, lime (usually as relicts in $Ca(OH)_2$ or CaS) was mainly found in modern CM objects such as burnt coal dumps. It enters unusual mineral assemblages found in calcined fragments of carbonate-petrified wood with the development of nut-like aggregates having a dense anhydrite shell and a friable core. Depending on the type of primary carbonates (calcite, dolomite, ankerite or siderite), the core consists either of a fine-grained aggregate of ferropericlase ((Mg,Fe)O), magnesioferrite ($MgFe_2O_4$), Ca-ferrites, hematite, fluormayenite or chlormayenite, and lime partially converted into oldhamite or portlandite, sometimes with larnite or spurrite. The anhydrite shell includes fluorapatite or fluorellestadite, chondrodite, fluorite, forsterite, anorthite, and wollastonite. Lime produced by calcite and/or dolomite calcination is

a precursor phase for anhydrite ($CaSO_4$), fluorite, $CaCl_2$, and oldhamite formed during gas-transport reactions commonly leading to total CaO consumption (Chesnokov and Tsherbakova 1991; Chesnokov et al. 1998; Sokol et al. 2002, 2005; Zateeva et al. 2007; Grapes 2011; Kokh et al. 2015).

Khoury et al. (2015) found only single ≤10 μm grain of lime partly converted to CaS or $Ca(OH)_2$ in natural CM marble of central Jordan (Table 2).

Lime and monteponite are obviously very rare minerals that occur in quite different geological environments and explain why naturally occurring CaO-CdO solid solutions have not been discovered before, though their presence is possible crystallochemically. CdO, ZnO, and $Ca_xCd_{1-x}O$ solid solutions are easily synthesized under dry high temperature – ambient pressure conditions and are largely utilized for making oxide wide bandgap semiconductors and materials for optical and electronic applications (Yogeeswaran et al. 2006; Duan et al. 2008; Srihari et al. 2011; Bakke et al. 2013; Chandiramouli and Jeyaprakash 2013). Intermediate members of the CaO-CdO series are formed in natural processes due to a unique, local combination of protolith geochemistry and Quaternary combustion metamorphism.

Protolith of Cd-rich combustion metamorphic marble

The Belqa Gr. sediments acquired abnormal trace element enrichments during deposition in an upwelling zone, as one may infer from relative contents of indicator elements (higher P and Cd and lower Co and Mn in the sediments and in products of their CM alteration (Delgadillo-Hinojosa et al. 2001; Brumsack 2006; Abed et al. 2005; Abed 2012; Abed and Sadaqah 2013). However, according to Fleurance et al. (2013), the abnormal Cr, Zn, and Ni enrichment, high Cd concentrations, and especially high Cd/Zn ratios (up to 1.88) in the Belqa Gr. sediments are far beyond those reported for such depositional environments and require a different explanation. Fleurance et al. (2013) attributed the accumulation of trace elements in the Belqa sediments to primary precipitation either from normal sea water during sedimentation or from sea water contaminated by an exogenic metal source, which was derived from hydrothermal fluids and/or enriched with an exogenic metal flux leached from ophiolites. The latter belong to the Baer Bassit (north-western Syria) and Troodos (Cyprus Island) syn-sedimentary island arc complexes located farther in the north. Additionally, Fleurance et al. (2013) invoked a hypothesis of epigenetic metal enrichment of buried sediments from diagenetic fluids akin to Mississippi Valley Type (MVT) deposits.

Sample DOS-1 from the Maastrichtian-Paleocene Muwaqqar Formation chalks contains more Cd (224 ppm) than the average (197.14 ppm) reported by Fleurance et al. (2013). Cadmium is hosted chiefly by (Zn,Cd)S: wurtzite $(Zn_{0.88}Cd_{0.08}Fe_{0.01}Cu_{0.01})_{\Sigma=0.99}S_{1.01}As_{0.01}$ and sphalerite $(Zn_{0.88}Cd_{0.07}Fe_{0.01}Cu_{0.01})_{\Sigma=0.97}S_{1.03}$). The highest Cd content reaches 9.6 wt% and 9.2 wt%, respectively,

that is above the maximum Cd concentrations in sphalerites from MVT deposits (Schwartz 2000; Ye et al. 2012). This is additional proof that the Late Cretaceous – Early Tertiary Belqa Gr. shallow marine sediments are young fresh equivalents of ancient carbonate sediments which became sources of Zn and Cd mineralization during the formation of MVT deposits, such as the Niujiaotang deposit in China (Ye et al. 2012). In the Dead Sea region, the Muwaqqar Fm. bitumen-rich chalky and marly sediments store the highest concentrations of Cd (197.14 ppm). Average Cd contents in the CM marbles and in the Muwaqqar Fm. limestones are, respectively, 129.80 ppm and 42.14 ppm (Fleurance et al. 2013). Cd contents vary from 1.3 to 73.6 ppm in phosphorites of the Transjordanian Plateau (Abed and Sadaqah, 2013) and are 22-43 ppm in the adjacent Negev desert phosphorites (Nathan et al. 1997).

Sedimentary parent rocks in different complexes from the Mottled Zone had notable enrichments in P, S, F and trace elements (U, Zn, Ni, Ba, Cr) inherited by their CM counterparts and, correspondingly, contained minerals that can concentrate these elements (Gross 1977; Techer et al. 2006; Fourcade et al. 2007; Milodowski et al. 2011; Sokol et al. 2011, 2014; Fleurance et al. 2013; Galuskin et al. 2013, 2014; Khoury and Al-Zoubi 2014; Khoury et al. 2011, 2014a,b,c, 2015). The marbles of the Tulul Al Hammam area produced by CM alteration of the Muwaqqar Fm. 'oil shales' are particular in this respect as they have high Cd/Zn ratios (0.185 on average) besides abnormal Cd enrichment (Table 1).

Conditions for the formation of CaO-CdO solid solutions in nature

The fine-grained Cd-bearing marbles rich in phosphorus and trace elements are ordinary CM rocks produced by subsurface combustion of bitumen matter and disseminated sulfides of the Muwaqqar Fm. Chalky sediments at medium temperatures (T_{max} = 800-850 °C), as reconstructed by Khoury et al. (2015). Most marbles in the Tulul Al Hammam area were calcined at high fuel/oxidizer ratios and bear Zn, Cd, Ni, Cu, Fe, Ag, Pb and Ca sulfides. Cadmium in these rocks is concentrated in abundant sphalerite (≤ 1.7 wt% CdO).

Intermediate members of the CaO-CdO solid solutions were discovered only in a few samples of CM marbles with a particular assemblage of accessory oxides. They are characterized by the (i) absence or rare presence of sulfide grains (detected only in sample TH-11); (ii) presence of simple and complex Ni, Zn, Cd, and Cu oxides, as well as (Mg,Zn,Ni,Cu)O solid solutions; (iii) stoichiometric Ca-U^{6+} oxides (Khoury et al. 2015) (Table 2). Fluorellestadite or (rarely) $(SO_4)^{2-}$-bearing fluorapatite, which point to oxidative conditions, are rock-forming minerals in these marbles. At free oxygen access to the combustion zone, sulfur (S^{2-}) from disseminated sulfides and organic matter oxidized to S^{6+} to form high-temperature complex sulfates, such as ternesite ($Ca_5(SiO_4)_2(SO_4)$), sulfate-rich apatite, and fluorellestadite (Parat et al. 2002; Zateeva et al. 2007; Milodowski et al. 2011; Marks et al. 2012; Kokh

et al. 2014; Khoury et al. 2015). Thus, the main phases bear signature of combustion metamorphism under oxidizing conditions, while the diverse accessories reflect local heterogeneity in trace-element loading of the protolith. There is petrographic evidence that, the marbles and/or their accessory minerals have formed by solid-state reactions.

Inasmuch as the CaO-CdO and ZnO-CdO systems are of special theoretical and practical interest (their members exhibit semiconductive properties), the conditions at which lime-monteponite ss form in nature can be checked against data on synthesis of their analogs (Miloua et al. 2008; Nazir et al. 2009; Srihari et al. 2011). Solid solutions of $Cd_{1-x}Ca_xO$ with x = 0.0-1.0 result from a solid state reaction, with CdO and CaO as starting materials. The procedure is as follows (Srihari et al., 2011): mixed powders are heat treated for 24 hours at 800 °C for samples with 5-10 at % Ca, at 900 °C for samples with 20-40 at % Ca, and at 1100 °C for other Ca-richer samples. $CaCdO_2$ compounds together with CuO are obtained by high-temperature solid state reactions at ambient pressure in oxygen atmosphere as synthesis byproduct of $CdBa_2CaCu_2O_y$ superconducting phases (Balchev 1994).

Given that sphalerite and wurtzite are main Cd concentrators in the parent sediments, it is also pertinent to consider the conversion of CdS into CdO. In experiments reported by Sebastian and Calixto (2000), CdS sintering in air (1 hour duration) led to a two-stage solid state reaction and formation of CdO at the CdS surface: $CdS + 2O_2 \rightarrow CdSO_4 \rightarrow CdO + SO_3$. The intermediate phase $CdSO_4$ arises at 300 °C, but breaks down at 400 °C and fully disappears at 500 °C. The XRD reflections corresponding to CdO start to appear at 400°C; at a higher temperature (500°C), they become intense and the CdS films eventually convert to a mixture of CdS and CdO phases.

Cadmium retention in high-temperature minerals

Unlike zinc, cadmium is among the trace elements that are preferentially released as a gas phase during decarbonation and, as a result, are hardly incorporated into the main OPC clinker phases (Achternbosch et al. 2003; Yang et al. 2014). Mineral assemblages of CM marbles correspond to early decarbonation of raw material during OPC clinker production: spurrite-fluormayenite/chlormayenite-brownmillerite-periclase without larnite (Ca_2SiO_4) and hatrurite (Ca_3SiO_5). The Cd-bearing mineral phases in these assemblages have implications for Cd retention in natural rocks for geological-scale periods of time and for long-term Cd mobility.

It is reasonable to begin with the available data on the incorporation of Cd into different crystalline phases of OPC clinkers. Like many other compounds of cadmium, its oxide is volatile (Lamoreaux and Hildebrand 1987). At high contents of CdO (up to 1 wt. %) added into raw mixes, the CdO incorporation ratio in OPC clinkers is 74-51 rel. % (Sprung 1985; Barros et al. 2004), while Cd becomes fully incorporated at 0.05 and 0.10 wt. % CdO. In presence of Cl, Cd is volatilized as $CdCl_2$,

strongly reducing incorporation (Barros et al. 2004). According to Murat and Sorrentino (1996), only 22 % Cd is trapped in Portland cement mainly as isomorphic impurity in CaO. Achternbosch et al. (2003) consider the (Ca,Cd)O phase to be the only Cd concentrator.

The mode of Cd occurrence in OPC clinker was studied by Yang et al. (2014) for experimental mixtures calcined in furnace at 1450°C for 1 hour. The relative percentages of main and accessory phases in these OPC clinkers were: 61.2 % alite (C_3S, Ca_3SiO_5), 21.5 % belite (C_2S, Ca_2SiO_4) 9.8 % brownmillerite, 4.0 % mayenite, 2 % lime (CaO free), and 1.2 % (Mg,Ni)O solid solutions. Cadmium was added to the raw mix as 1 wt% of CdO, and cadmium contents of OPC clinker product phases were assessed by EPMA. Cadmium was identified only in C_3S (0.33-1.08 wt% CdO, isomorphic substitution), brownmillerite (0.60-1.47 wt% CdO, interstitial solid solutions), and in the CaO phase (1.83-7.97 wt% CdO as a Ca-Cd-O sosoloid (solid particles dispersed in another solid)).

The distribution of Cd^{2+} in OPC clinker mineral assemblages is generally controlled by crystallochemistry. There is isomorphic substitution of Cd^{2+} ($r^{[6]} = 0.95$ Å) for Ca^{2+} ($r^{[6]} = 1.00$ Å), while the (Ca,Cd)O ss has the highest incorporation ratio. The case of CM marbles from central Jordan provides another illustration for this conclusion. The marbles formed at much lower temperatures than OPC clinkers and thus lack hatrurite (a natural analog of alite). As for other OPC clinker phases, Cd is below the detection limit (< 0.07 wt% CdO) in spurrite, mayenite supergroup minerals, and brownmillerite but is high in some accessory oxides, which allows calculation of their respective incorporation ratios (Table 6).

Intermediate members of lime-monteponite solid solution series. The $(Ca_{0.645}Cd_{0.355})O$ – $(Ca_{0.453}Cd_{0.547})O$ phase stores most of cadmium in CM marbles (58.54 wt% ≤ CdO ≤ 73.25 wt%), with the average incorporation ratio $K_{Cd} = 843$, but contains very little Zn (0.75 wt% ZnO_{max}; $K_{Zn} \leq 5.2$). Our results for a natural single crystal of $(Ca_{0.49}Cd_{0.51})O$ are fully consistent with the earlier inference that $Ca_xCd_{1-x}O$ ($0 \leq x \leq 1$) is a solid solution series with the NaCl-type crystal structure (Murtaza et al. 2012). The atomic positions of Ca and Cd are mixed, without evident cation ordering (Table 4). No solid particles (CdO) dispersed in another solid (CaO), like those found by (Yang et al. 2014), have been detected in natural minerals formed under long-term heating.

Zincite (wurtzite-type structure) has the highest average Zn incorporation ratio ($K_{Zn} = 525.6$), while the content of CdO ≤ 3 wt%. However, $K_{Cd} \leq 37.6$, and, according to the criterion of Achternbosch et al. (2003), zincite in natural marbles is likewise a phase providing efficient Cd retention.

Tululite, a complex oxide of Ca, Al and Zn, incorporates both Cd and Zn, with the respective average ratios $K_{Cd} = 107.3$ and $K_{Zn} = 121.4$, due to its structure in which Cd^{2+} substitutes for Ca^{2+} in a trigonal prismatic coordination and average interatomic distances are M–O = 2.34 – 2.51 Å. Zn^{2+} is

present in amounts commensurate with Al^{3+} and occupies the proper tetrahedral sites with a mean interatomic distance of T – O = 1.97 Å. The mineral is a common accessory in the studied rocks; although the Cd contents are moderate (5-8.5 wt% of CdO), the total amount of bound Cd may be rather high. Other compounds proximal to tululite, which were inferred to be Zn immobilizers (Gineys et al. 2011a,b), may incorporate Cd to a large probability.

Periclase, the second widespread accessory mineral with NaCl-type crystal structure, accumulates large percentages of ZnO (23 wt%, with K_{Zn} = 128.6 on average), contains Ni and Cu but lacks Cd.

Thus, the multi-component Ca-dominated system such as CM marbles contains Cd mainly in the form of $(Ca_xCd_{1-x})O$ solid solutions. This phase resulted from oxidative calcination of marine carbonate sediments prior to clinkering (as indicated by calcite-spurrite assemblages). Tululite is another concentrator of Cd, with Cd^{2+} substituting for Ca^{2+}in the structure. Cadmium is incorporated into the wurtzite-type structure of ZnO in minor amounts but lacks from the NaCl-type structure of MgO. The steric factor in natural assemblages impedes the formation of Cd-doped MgO ($r^{[6]}$ Mg^{2+} 0.72 Å) and ZnO ($r^{[4]}$ Zn^{2+} 0.60 Å) in the presence of Ca phases ($r^{[6]}$ Ca^{2+} 1.00 Å), which are more favorable for incorporation of Cd ($r^{[6]}$ Cd^{2+} 0.95 Å).

Cadmium retention in supergene environments

The mechanism of cadmium immobilization and the influence of Cd on cement hydration remain poorly understood, though it has been the subject of several publications. According to the review of Achternbosch et al. (2003), the behavior of Cd in the hydrated young cement pastes depends on the presence of dissolved salts (chlorides and/or sulfates). In their absence, under alkaline conditions (8 < pH < 12.5), Cd mainly exists as insoluble hydroxides produced by primary hydration, as carbonate or as non-hydraulic minor phases. Incorporation of cadmium as insoluble hydroxides was inferred to provide effective Cd retention (Cartledge et al. 1990; Pomiès et al. 2001a,b), while Herrera et al. (1992) suggested formation of mixed Ca-Cd hydroxides or calcium hydrocadmiates, $CaCd(OH)_4$. Achternbosch et al. (2003) also noted that Cd hydroxide precipitation was related with $Ca(OH)_2$. The retardant effect from the presence of Cd in the system was explained (Mollah et al. 1995) by the formation of calcium hydrocadmiate as a result of the reaction between $Cd(OH)_4^{2-}$ and Ca^{2+} that coat the CSH surface.

The data we obtained for natural assemblages agree well with the results of Pomiès et al. (2001a, b) that Cd speciation in hydrated cement systems is not a simple precipitation of $Cd(OH)_2$, which has low solubility ($K_{sp} = 10^{-13.7}$). Alkaline suspensions (high water/solid ratio) and cement pastes (low water/solid ratio) have different mechanisms of cadmium fixation (Cartledge et al. 1990;

Herrera et al. 1992; Diez et al. 1997; Achternbosch et al. 2003). In the case of cement paste, $Cd(OH)_2$ precipitation has never been observed but $(Ca_{1-x}Cd_x)(OH)_2$ solid solutions (with *x* up to 0.5) can form. The wide compositional range of solid solutions does not depend on the initial cadmium content and reflects the chemical composition heterogeneity of the system.

The hydration degree of high-temperature phases is the lowest in fine-grained hard marbles (sample DT-7). The cores of spurrite and chlormayenite grains remain fresh and are coated with hydrated rims, while periclase and brownmillerite grains are fresh over the greatest part. The degree of secondary carbonation of CSHs is negligible. Hydration occurred upon percolation of meteoric water film into thin cracks between grains, which defined very low water/solid ratios. Coarse grains (Ca,Cd)O in these rocks are always covered with a dense coat of $(Ca_{1-x}Cd_x)(OH)_2$ solid solutions (x = 0.36-0.55). According to the IMA-CNMNC rule (Hatert and Burke 2008), the mineral with x = 0.36-0.50 should be named Cd-rich portlandite, whereas the phase with x = 0.51-0.55 can be treated as a new mineral species. The Ca/Cd ratio in Cd-rich portlandite corresponds to this ratio in the primary oxide. No Cd leakage from these grains has been observed (Figs. 4d, 5 and 6d; Table 5). During the preparation of thin sections, perfectly fresh micrometer grains of (Ca,Cd)O were brought out, which were located inside non-cracked calcite crystals (Figs 6e-f). No otavite (Cd carbonate) has been found.

The set of secondary products is different in the sample TH-72, a rock altered by Cl^-- and F^--bearing solutions. Altered (Ca,Cd)Oss grains are surrounded by a halo of Cd and /or Cl-bearing phases produced by fluid infiltration along cracks. Cadmium is also accumulated in CSHs aggregates (8-19 wt%, rarely up to 38 wt% CdO). The mechanism of such Cd immobilization has not been reconstructed yet. By analogy with processes discussed by Pomiès et al. (2001a, b), Cd sorption onto the CSH surface or Ca-Cd exchange between already formed CSHs and Cd-rich chloride solutions appear to be likely candidates.

It is hardly possible to rigorously constrain the compositions of Cl- and/or F-bearing cadmium secondary phases. Effective separation of Ca and Cd is provided by strongly different solubilities of their fluorides: CaF_2 (0.0016 g/100 g H_2O, T = 18 °C) and CdF_2 (4.5 g/100 g H_2O, T = 25 °C) (Linke and Seidell 1965), while Ca is fixed as fluorite. The relations of Cd, O, and Cl determined by EDS allow classifying secondary compounds as basic cadmium chlorides $(Cd(OH)_{2-x}Cl_x)$, which are stable in aqueous NaCl solutions and isostructural with $Cd(OH)_2$ (Janusz 1991). The most probable scenario is the formation of thin mixed and/or laminated aggregates of basic cadmium chlorides with fluorite. A simpler case of a (Ca,Cd)O core coexisting with a zoned fluorite and Cd-rich portlandite $(Ca,Cd)(OH)_2$ rim is shown in Fig. 10 and Table 5 (sample TH-18).

Time and climate: how representative are the data obtained for the Transjordanian Plateau?

The knowledge coming from geological sites where rocks have been exposed to chemical weathering for about ~ 100 ka is of exceptional value for long-term predictions for the retention of toxic compounds (Achternbosch et al. 2003; Yang et al. 2014). The duration of this weathering has not been estimated directly in the Tulul Al Hammam area, but such estimates are available for the neighbor Khushaym Matruk area of the CM Siwaqa complex (Techer et al. 2006). Using the U–Th disequilibrium method, Techer et al. (2006) evaluated that intense alteration of CM rocks in the course of repeated reactivation of cracks with multiphase paleo-circulations of alkaline fluids occurred 110,000–130,000 years ago. A similar approach performed on samples from veins crosscutting the CM marbles at the Maqarin complex in north Jordan gives ages around 80 – 160 ka (Alexander and Smellie 1998). Some scenario of this kind may have acted in the Tulul Al Hammam area as well.

Besides time, climate is another important control of the mobility of elements leached from rocks and disposal sites. The present climate of the Transjordanian Plateau is arid to hyper-arid (110 mm of annual precipitation, mean summer temperature of 23 °C with a maximum of 44 °C and high evaporation). However, the 350 ka climate record of the southern Levant holds evidence of much wetter conditions in the past, with local moist episodes, mainly during glacial periods. According to paleoclimate reconstructions using calcite speleothems in arid and hyper-arid rain-shadow areas surrounding the Dead Sea (Lisker et al. 2010; Vaks et al. 2010), major humid periods in the area for the past 350 ka occurred at 350–310 ka, 310–290 ka, 220–190 ka, and 142–109 ka. Therefore, data on Cd fixation in Jordanian CM marbles have implications for calcination-induced Cd immobilization, as well as for long-term Cd retention during cement hydration in a wetter climate.

IMPLICATIONS

The spurrite-fluorellestadite (±sulfate-fluorapatite, brownmillerite, fluormayenite, chlormayenite) marbles from central Jordan were produced by medium-temperature combustion metamorphism of calcareous marine sediments, notably bitumen-rich impure chalks of the Muwaqqar Chalk Marl Formation enriched in Zn, Ni, Cd, and U. The sedimentary protolith of the CM marbles contains abundant Cd-rich wurtzite and sphalerite (Cd/Zn ~ 0.15), which became the main source of Cd for CM oxide mineralization. In the Quaternary, the chalky sediments exposed to surface effects were heated to 800-850 °C. Some of them were sintered in the conditions of oxidizer excess relative to fuel (dispersed bitumen and sulfides). Thus, $(Zn,Cd)S_{ss}$ phases burnt out during chalk calcination, Cd became fractionated from Zn, and the elements were accumulated in different oxide accessories: lime-monteponite solid solutions ((Ca,Cd)O), Ca and Zn aluminate, tululite $(Ca,Cd)_{14}(Fe^{3+},Al)(Al,Zn,Fe^{3+},Si,P,Mn,Mg)_{15}O_{36}$), zincite (ZnO), and periclase (Mg,Zn,Ni,Cu)O. Prior

to complete clinkering (spurrite- and calcite-bearing assemblages), Cd incorporation into different oxides was controlled by steric factor at predominant $Cd^{[6]} \rightarrow Ca^{[6]}$ isomorphic substitution. The intermediate members of the lime-monteponite solid solutions $(Ca_{0.645}Cd_{0.355})O - (Ca_{0.453}Cd_{0.547})O$ with a NaCl-type structure and a cadmium incorporation ratio ($K_{Cd} = Cd_{mineral}/Cd_{rock}$) of ~ 843 are chief hosts for cadmium in CM marbles. Thus, Cd and Zn fractionation and formation of independent Cd mineralization may occur in both supergene and high-temperature-low-pressure oxidative environments.

Cadmium immobilization in natural rocks in supergene environments strongly depends on water/rock ratios and the presence of Cl^- and F^- in solutions, which fully agrees with data obtained for cement systems (Pomiès et al. 2001b; Achternbosch et al. 2003). At low water/rock ratios, $(Ca_{1-x}Cd_x)(OH)_2$ ss (*x* up to 0.55) is the main natural secondary phase after (Ca,Cd)O ss. However, calcium and cadmium can precipitate as separate phases of fluorite and basic cadmium chlorides $(Cd(OH)_{2-x}Cl_x)$ at higher water/rock ratios and in the presence of Cl^- and F^-. In the same conditions, cadmium becomes fixed in CSHs.

The findings of numerous $(Ca,Cd)O_{ss}$ grains partly substituted by $(Ca_{1-x}Cd_x)(OH)_2$ solid solutions in naturally occurring rocks subjected to chemical weathering for at least 100 ka proves high efficiency of both phases as Cd immobilisers. The coexisting grains of Cd-bearing zincite and tululite remain fresh and are free from hydration signatures. Therefore, the two phases can retain both Cd and Zn for long periods of time. Thus, natural analogs of cement-like matrix occur also in the Tulul Al Hammam area which is another exceptional geological site of this kind in Jordan, along with the well-known Maqarin site (Alexander et al. 1992, Clark et al. 1992, Khoury et al. 1992, Alexander and Smellie 1998), the Khushaym Matruk site (Techer et al. 2006; Elie et al. 2007; Fourcade et al. 2007; Khoury et al. 2011; Milodowski et al. 2011).

ACKNOWLEDGEMENTS

The manuscript profited much from the thoughtful review and valuable comments by Professor Maarten Broekmans, Associated Editor of American Mineralogist, which we have accepted with gratitude, as well as the comments by anonymous reviewers. The first author would like to thank the Deanship of Scientific Research at the University of Jordan for their support during his sabbatical year 2012/2013 at the Department of Earth Sciences, University of Ottawa, Canada. Thanks are extended to Late Prof. Andre Lalonde for his participation in the University of Ottawa collaboration. Thanks are also given to Tara Kell (XRD lab), and Glenn Poirier (MicroAnalysis Lab.) and to Drs. N. Karmanov, E. Nigmatulina, and M. Khlestov (IGM, Novosibirsk) for assistance during the analytical work. Wadah Faris, Yousef Abu Salheh, and Azzam Azzarah (University of Jordan, Amman) are acknowledged for

their help in the field and in preliminary studies. T. Perepelova (IGM, Novosibirsk) is thanked for helpful advice to the present work. Trace element abundances were analyzed by Yu. Kolmogorov at the shared-research Siberian Synchrotron and Terahertz Radiation Centre, Budker Institute of Nuclear Physics (Novosibirsk, Russia). The Russian contribution was supported by grant 15-05-00760 from the Russian Foundation for Basic Research.

REFERENCES

Abed, A.M., Arouri, K.R., and Boreham, C.J. (2005) Source rock potential of the phosphorite-bituminous chalk-marl sequence in Jordan. Marine and Petroleum Geology, 22, 413–425.

Abed, A. (2012) Review of uranium in the Jordanian phosphorites: Distribution, genesis and industry. Jordan Journal of Earth and Environmental Sciences, 4, 35–45.

Abed, A., and Sadaqah, R. (2013) Enrichment of uranium in the uppermost Al-Hisa Phosphorite Formation, Eshidiyya basin, southern Jordan. Journal of African Earth Sciences, 77, 31–40.

Achternbosch, M., Bräutigam, K.-R., Hartlieb, N., Kupsch, C., Richers, U., and Stemmermann, P. (2003) Heavy metals in cement and concrete resulting from the co-incineration of wastes in cement kilns with regard to the legitimacy of waste utilization, 200 p. Forschungszentrum Karlsruhe in der Helmholtz-Gemeinschaft Wissenschaftliche Berichte FZKA 6923. Umwelt Bundes Amt. Germany. On line at: http://www.coprocem.com/documents/uba_karlsruhe.pdf

Alexander, W.R., and Smellie, J.A.T. (1998) Maqarin natural analogue project: ANDRA, CEA, NAGRA, NIREX and SKB synthesis report on phases I, II and III. 101 p. Scientific Technical Report NPB 98-08. Nagra, Wettingen, Switzerland.

Alexander, W.R., Dayal, R., Eagleson, K., Eikenberg, J., Hamilton, E., Linklater, C.M., McKinley, I.G., and Tweed, C.J. (1992) A natural analogue of high pH cement pore waters from the Maqarin area of northern Jordan II: results of predictive geochemical calculations. Journal of Geochemical Exploration, 46, 133–146.

Bakke, J.R., Hägglund, C., Jung, H.J., Sinclair, R., and Bent, S.F. (2013) Atomic layer deposition of CdO and $Cd_xZn_{1-x}O$ films. Materials chemistry and Physics, 140, 465–471.

Balchev, N. (1994) Superconductivity in Cd-Ba-Ca-Cu-O system. Applied Superconductivity, 2 (6), 435–436.

Barros, A.M., Tenório, J.A.S., and Espinosa, D.C.R. (2004) Evaluation of the incorporation ratio of ZnO, PbO and CdO into cement clinker. Journal of Hazardous Materials, B112, 71–78.

Bender, F. (1968) Geologie von Jordanien. Beiträge zur Regionalen Geologie der Erde, Band 7. Gebrüder Bornträger; Berlin.

Bowen, N.L. (1940) Progressive metamorphism of siliceous limestone and dolomite. Journal of Geology, 48, 225–274.

Brese, N.E., and O'Keeffe M. (1991) Bond-valence parameters for solids. Acta Crystallographica, B47, 192-197.

Brumsack, H.-J. (2006) The trace metal content of recent organic carbon-rich sediments: implications for Cretaceous black shale formation. Palaeogeography, Palaeoclimatology, Palaeoecology, 232, 344-361.

Cartledge, F.K., Butler, L.G., Chalasani, D., Eaton, H.C., Frey, F.P., Herrera, E., Tittlebaum, M.E., and Yang, S.-L. (1990) Immobilization mechanisms in solidification/stabilization of Cd and Pb salts using Portland cement fixing agents. Environmental Science and Technology, 24, 867–873.

Chandiramouli, R., and Jeyaprakash, B.G. (2013) Review of CdO thin films. Solid State Sciences, 16, 102–110.

Chaplygin, I.V., Mozgova, N.N., Bryzgalov, I.A., and Mokhov, A.V. (2004) Cadmoindite, $CdIn_2S_4$, a new mineral from Kudriavy volcano, Iturup Isle, Kurily Islands. Zap. Vses. Mineral. Obshchest., 133 (4), 21–27 (in Russian).

Chaplygin, I.V., Mozgova, N.N., Bryzgalov, I.A., Makovicky, E, Balic-Zunic, T., Magazina, L.O., Kuznetsova, O.Yu., and Safonov, Yu.G. (2005) Kudriavite $(Cd,Pb)Bi_2S_4$, a new mineral species from Kudriavy volcano, Iturup Island, Kuriles. Canadian Mineralogist, 43, 695–701.

Chaplygin, I.V., Mozgova, N.N., Mokhov, A.V., Koporulina, E.V., Bernhardt, H.-J., and Bryzgalov, I.A. (2007) Minerals of the system ZnS–CdS from fumaroles of the Kudriavy volcano, Iturup Island, Kuriles, Russia. Canadian Mineralogist, 45, 709–722.

Chesnokov, B., Kotrly, M., and Nisanbajev, T. (1998) Brennende Abraumhalden und Aufschlüsse im Tscheljabinsker Kohlenbecken - eine reiche Mineralienküche. Mineralien-Welt, 9 (3), 54–63 (in German).

Chesnokov, B.V., and Shcherbakova, E.P. (1991) Mineralogy of the burnt dumps of the Chelyabinsk Coal Basin: an experience in technogenic mineralogy, 152 p. Nauka, Moscow (in Russian).

Clark, I.D., Fritz, P., Milodowski, A.E., and Khoury, H.N. (1992) Sampling and analytical methods in: A natural analogue study of the Maqarin hyperalkaline groundwaters. Nagra Technical Report 91-10, Wettingen, Switzerland, pp. 19–40.

Delgadillo-Hinojosa, F., Macías –Zamora, J.V., Segovia-Zavala, J.A., and Torres-Valdés, S. (2001) Cadmium enrichment in the Gulf of California. Marine Chemistry, 75, 109-122.

Deer, W.A., Howie, R.A., and Zussman, J. (1992) An introduction to the rock forming minerals. 2nd excerpted student edition, 696p. Longman, Burnt Mill.

De Waele, J., Forti, P., and Naseddu, A. (1999) Le "Grotte di Miniera": patrimonio scientifico e risorsa turistica in: Atti del Convegno Internazionale di Studio "Paesaggio Minerario" Cagliari, 7-10 Ottobre 1999; abstracts.

De Waele, J., and Forti, P. (2005) Mineralogy of mine caves in Sardinia (Italy) in: The 14th International Congress of Speleology, Kalamos, Greece; abstracts. Proceedings Volume, 306–311

Diez, J.M., Madrid, J., and Macias, A. (1997) Characterization of cement-stabilized Cd wastes. Cement and Concrete Research, 27, 337–343.

Dobbe, R.T.M. (1992) Manganoan–cadmian tetrahedrite from the Tunaberg Cu–Co deposit, Berglagen, central Sweden. Mineralogical Magazine, 56, 113–115.

Duan, Y., Qin, L., Tang, G., and Shi, L. (2008) First-principles study of ground- and metastable-state properties of XO (X = Be, Mg, Ca, Sr, Ba, Zn and Cd). The European Physical Journal B, 66, 201-209.

Elie, M., Techer, I., Trotignon, L., Khoury, H., Salameh, E., Vandamme, D., Boulvais, P., and Fourcade, S. (2007) Cementation of kerogen-rich marls by alkaline fluids released during weathering of thermally metamorphosed marly sediments. Part II: Organic matter evolution, magnetic susceptibility and metals (Ti, Cr, Fe) at the Khushaym Matruck natural analogue (central Jordan). Applied Geochemistry, 22, 1311–1328.

Fadeeva, V.P., Tikhova, V.D., and Nikulicheva, O.N. (2008) Elemental analysis of organic compounds with the use of automated CHNS analyzers. Journal of Analytical Chemistry, 63(11), 1094–1106.

Fleurance, S., Cuney, M., Malartre, M., and Reyx, J. (2013) Origin of the extreme polymetallic enrichment (Cd, Cr, Mo, Ni, U, V, Zn) of the Late Cretaceous–Early Tertiary Belqa Group, central Jordan. Palaeogeography, Palaeoclimatology, Palaeoecology, 369, 201–219.

Fleischer, M. (1966) New mineral names. American Mineralogist, 51, 1815-1820.

Fiquet, G., Richet, P., and Montagnac, J. (1999) High-temperature thermal expansion of lime, periclase, corundum and spinel. Physics and Chemistry of Minerals, 27, 103–111.

Forti, P. (1985) Alcuni nuovi minerali carsici dell'Iglesiente. Notiziario di Mineralogia e Paleontologia, 44, 3–10.

Forti, P., and Perna, G. (1988) Genesi della monteponite di Monteponi. Rivista Italiana di Mineralogia, 1, 45–51.

Fourcade, S., Trotignon, L., Boulvais, P., Techer, I., Elie, M., Vandamme, D., Salameh, E., and Khoury, H. (2007) Cementation of kerogen-rich marls by alkaline fluids released during weathering of thermally metamorphosed marly sediments. Part I: Isotopic (C, O) study of the Khushaym Matruk natural analogue (central Jordan). Applied Geochemistry, 22, 1293–1310.

Galuskin, E.V., Kusz, J., Armbruster, T., Galuskina, I.O., Marzec, K., Vapnik, Y., and Murashko, M. (2013) Vorlanite, ($CaU^{6+)}O_4$, from Jabel Harmun, Palestinian Autonomy, Israel. American Mineralogist, 98, 1938–1942.

Galuskin, E., Galuskina, I., Kusz, J., Armbruster, T., Marzec, K., Dzierżanowski P., and Murashko, M. (2014) Vapnikite Ca_3UO_6 – a new double-perovskite mineral from pyrometamorphic larnite rocks of the Jabel Harmun, Palestinian Autonomy, Israel. Mineralogical Magazine, 78, 571-581.

Galuskin, E.V., Gfeller, F., Galuskina, I.O., Armbruster, T., Bailau, R., and Sharygin, V.V. (2015) Mayenite supergroup, part I: Recommended nomenclature. European Journal of Mineralogy, 27, 99-111.

Gineys, N., Aouad, G., and Damidot, D. (2011a) Managing trace elements in Portland cement – Part II: Comparison of two methods to incorporate Zn in a cement. Cement and Concrete Composites, 33, 629-636.

Gineys, N., Aouad, G., Sorrentino, F., and Damidot, D. (2011b) Incorporation of trace elements in Portland cement clinker: Thresholds limits for Cu, Ni, Sn or Zn. Cement and Concrete Research, 41, 1177-1184.

Goryainov, S.V., Likhacheva, A.Y., Rashchenko, S.V., Shubin, A.S., Afanasiev, V.P., and Pokhilenko, N.P. (2014) Raman identification of lonsdaleite in Popigai impactites. Journal of Raman Spectroscopy, 45, 305–313.

Goryainov, S.V., Krylov, A.S., Pan, Yu., Madyukov, I.A., Smirnov, M.B., and Vtyurin, A.N. (2012) Raman investigation of hydrostatic and nonhydrostatic compressions of OH- and F-apophyllites up to 8 GPa. Journal of Raman Spectroscopy, 43, 439–447.

Grapes, R. (2011) Pyrometamorphism, second edition, 290 p. Springer, Berlin.

Gross, S. (1977) The mineralogy of the Hatrurim Formation, Israel. Geological Survey of Israel Bulletin, 70, 1–80.

Hatert, F., and Burke, E.A.J. (2008) The IMA-CNMNC dominant-constituent rule revisited and extended. Canadian Mineralogist, 46, 717-728.

Herrera, E., Tittlebaum, M., Cartledge, F., and Eaton, H. (1992) Evaluation of the leaching properties of solidified heavy metal wastes. Journal of Environmental Science and Health, Part A, 27 (4), 983–998.

Humphries, D.W. (1992) The preparation of thin sections of rocks, minerals and ceramics. p83. Royal Microscopical Society, Oxford Science Publications, Microscopy Handbooks (24).

Janusz, W. (1991) Adsorption and Precipitation Processes in the Cadmium Oxide/Aqueous NaCl or $NaClO_4$ Solution System. Journal of Colloid and Interface Science, 145 (1), 119-126

Khoury, H. (2012) Long-term analogue of carbonation in travertine from Uleimat Quarries, central Jordan. Environmental Earth Sciences, 65, 1909-1916.

Khoury, H., Trotignon, L., Techer, I., Elie, M., Salameh, E., Bienvenu, P., Boulvais, P., Didot, A., Félines, I., Fontanini, L., Fourcade, S., Martinez, L., Parneix, J., Ramirez-Martin, S., Rassineux, F., Rayna, J., and Vandamme, D. (2011) Khushaym Matruk, Chapter 6 in *Pitty,* A. and Alexander, R., (Eds.), (2011). A natural analogue study of cement buffered, hyperalkaline groundwaters and their interaction with a repository host rock IV: an examination of the Khushaym Matruk (central

Jordan) and Maqarin (northern Jordan) sites. NDA-RWMD Technical Report, NDA, Moors Row, UK.

Khoury, H., and Nassir, S. (1982a) A discussion on the origin of Daba – Siwaqa marble. Dirasat, 9, 55-56.

Khoury, H., and Nassir, S. (1982b) High temperature mineralization in Maqarin area, North Jordan. Neues Jahrbuch für Mineralogie (Abhandlungen), 144, 197–213.

Khoury, H.N., Salameh, E., Clark, F., Fritz, R., Bajjali, W., Miolodwski, A., Cave, M., and Alexander, W. (1992) A natural analogue of high pH waters from the Maqarin area of northern Jordan 1: Introduction to the site. Journal of Geochemical Exploration, 46, 117–132.

Khoury, H.N., and Al-Zoubi, A.S. (2014) Origin and characteristics of Cr-smectite from Suweileh area, Jordan. Applied Clay Science, 90, 43–52.

Khoury, H., Salameh, E., and Clark, I. (2014a) Mineralogy and origin of surficial uranium deposits hosted in travertine and calcrete from central Jordan. Applied Geochemistry, 43, 49–65.

Khoury, H., Sokol, E., Kokh, S.N., and Clark, I. (2014b) High-temperature Cd-Ca oxide – the first finding in nature: case study in the varicolored marble of Jordan in: The International conference Humboldt Kolleg "Building International Network for Enhancement of Research in Jordan; abstracts. Abstract Volume, 156.

Khoury, H.N., Sokol, E.V., Kokh, S.N., Seryotkin, Y.V., Nigmatulina, E.N., Goryainov, S.V., Belogub, E.V., and Clark, I.D. (2014c) Tululite, IMA 2014-065. CNMNC Newsletter No. 23, February 2015, page 53; Mineralogical Magazine, 79(1), 51-58

Khoury, H., Sokol, E., and Clark, I. (2015) Calcium Uranium Oxides from Central Jordan: Mineral Assemblages, Chemistry, and Alteration Products. Canadian Mineralogist, 53 (1), DOI: 10.3749/canmin.1400071.

Kokh, S.N., Sokol, E.V., and Sharygin, V.V. (2015) Ellestadite-group minerals in combustion metamorphic rocks, Chapter 20 in Stracher, G. B., Prakash, A. & Sokol, E. V. (Eds.), Coal and Peat Fires: A global perspective, Elsevier, Amsterdam, 3, 543-562.

Korzhinsky, M.A., Tkachenko, S.I., Shmulovich, K.I., Taran, Y.A., and Steinberg, G.S. (2004) Discovery of a pure rhenium mineral at Kudriavy volcano. Nature, 369, 51-52.

Lamoreaux, R.H., and Hildebrand, D.L. (1987) High-temperature vaporization behavior of oxides II. Oxides of Be, Mg, Ca, Sr, Ba, B, Ga, In, Tl, Si, Ge, Sn, Pb, Zn, Cd and Hg. Journal of Physical and Chemical Reference Data, 16(3), 419-443.

Lisker, S., Vaks, A., Bar-Matthews, M., Porat, R., and Frumkin, A. (2010) Late Pleistocene palaeoclimatic and palaeoenvironmental reconstruction of the Dead Sea area (Israel), based on speleothems and cave stromatolites. Quaternary Science Reviews, 29, 1201–1211.

Linke, W.F., and Seidell, A. (1965) Solubilities of Inorganic and Metal Organic Compounds, 4th edition, 1070 p. American Chemical Society, Washington.

Marks, M.A.W., Wenzel, T., Whitehouse, M.J., Loose, M., Zack, T., Barth, M., Worgard, L., Krasz, V., Eby, G.N., Stosnach, H., and Markl, G. (2012) The volatile inventory (F, Cl, Br, S, C) of magmatic apatite: An integrated analytical approach. Chemical Geology, 291, 241–255.

Milodowski, A.E., Trotignon, L., Khoury, H., Salameh, E., Arnal, N., Bienvenu, P., Bulle, C., Chenery, S.R., Crouzet, N., Fontanini, L., Hodgkinson, E.S., Mäder, U., McKervey, J., Peycelon, H., Pontremol, S., Rassineux, F., Raynal, J., Rose, J., Vandamme, D., Provitina, O., and Raimbault, L. (2011) The analogue cement zone (ACZ), Chapter 4 in Pitty, A. & Alexander, R., (Eds.), A natural analogue study of cement buffered, hyperalkaline groundwaters and their interaction with a repository host rock IV: an examination of the Khushaym Matruk (central Jordan) and Maqarin (northern Jordan) sites. NDA-RWMD Technical Report, NDA, Moors Row, UK.

Miloua, R., Kebbab, Z., Miloua, F., and Benramdane, N. (2008) Ab initio investigation of phase separation in $Ca_{1-x}Zn_xO$ alloys. Physics Letters A, 372 (11), 1910–1914.

Mollah, M.Y.A., Vempati, R.K., Lin, T.C., and Cocke, D.L. (1995) The interfacial chemistry of solidification/stabilization of metals in cement and pozzolanic material systems. Waste Management, 15, 137–148.

Morgan, G.B., and London, D. (2005) Effect of current density on the electron microprobe analysis of alkali aluminosilicate glasses. American Mineralogist, 90, 1131-1138.

Murat, M., and Sorrentino, F. (1996) Effect of large additions of Cd, Pb, Cr, Zn, to cement raw meal on the composition and the properties of the clinker and the cement. Cement and Conacte Research, 26 (3), 377-385.

Murtaza, G., Amin, B., Arif, S., Maqbool, M., Ahmad, I., Afaq, A., Nazir, S., Imran, M., and Haneef, M. (2012) Structural, electronic and optical properties of $Ca_xCd_{1-x}O$ and its conversion from semimetal to wide bandgap semiconductor. Computational Materials Science 58, 71–76.

Nathan, Y., Soudry, D., Levy, Y., Shitrit, D., and Dorfman, E. (1997) Geochemistry of cadmium in the Negev phosphorites. Chemical Geology, 142, 87–107.

Nazir, S., Ikram, N., Amin, B., Tanveer, M., Shaukat, A., and Saeed, Y. (2009) Structural, electronic and optical calculations of $Ca_xZn_{1-x}O$ alloys: A first principles study. Journal of Physics and Chemistry of Solids, 70, 874–880.

Oxford Diffraction (2008) CrysAlisRED 171.37.35. Oxford Diffraction Ltd, Abingdon, England.

Papike, J.J. (1987) Chemistry of the rock-forming silicates: Ortho, ring, and single-chain structures. Reviews of Geophysics, 25(7), 1483-1526.

Papike, J.J. (1988) Chemistry of the rock-forming silicates: Multiple-chain, sheet, and framework structures. Reviews of Geophysics, 26(3), 407-444.

Parat, F., Dungan, M.A., and Streck, M.J. (2002) Anhydrite, pyrrhotite, and sulfur-rich apatite: tracing the sulfur evolution of an Oligocene andesite (Eagle Mountain, CO, USA). Lithos, 64, 63-75.

Pattrick, R.A.D. (1978) Microprobe analyses of cadmium-rich tetrahedrites from Tyndrum, Perhshire, Scotland. Mineralogical Magazine, 42, 286–288.

Pattrick, R.A.D., and Hall, A.J. (1983) Silver substitution into synthetic zinc, cadmium, and iron tetrahedrites. Mineralogical Magazine, 47, 441–451.

Phedorin, M.A., Bobrov, V.A., Chebykin, E.P., Goldberg, E.L., Melgunov, M.S., Filippova, S.V., and Zolotarev, K.V. (2000) Comparison of synchrotron radiation X-ray fluorescence with conventional techniques for the analysis of sedimentary samples. Journal Geostandards and Geoanalytical Research, 24, 205-216.

Pomiès, M.-P., Lequeux, N., and Boch, P. (2001a) Speciation of cadmium in cement: Part I. Cd^{2+} uptake by C-S-H. Cement and Concrete Research, 31, 563–569.

Pomiès, M.-P., Lequeux, N., and Boch, P. (2001b) Speciation of cadmium in cement: Part II. C_3S hydration with Cd^{2+} solution. Cement and Concrete Research, 31, 571–576.

Powell, J.H., and Moh'd, B.K. (2011) Evolution of Cretaceous to Eocene alluvial and carbonate platform sequences in central and south Jordan. GeoArabia, 16, 29–82.

Rieder, K.H., Weinstein, B.A., Cardona, M., and Bilz H. (1973) Measurement and comparative analysis of the second-order Raman spectra of the alkaline-earth oxides with a NaCl structure. Physical Review B, 8, 4780–4786.

Rudnick, R.L., and Gao, S. (2003) Composition of the continental crust. In: Rudnick R.L. (ed) The crust. Treatise on geochemistry 3, Elsevier, Amsterdam, 1–64.

Schwartz, M.O. (2000) Cadmium in zinc deposits: economic geology of a polluting element. International Geology Review, 42, 445–469.

Shatsky, V.S., Sitnikova, E.S., Koz'menko, O.A., Palessky, S.V., Nikolaeva, I.V., and Zayachkovsky, A.A. (2006) Behavior of incompatible elements during ultrahigh-pressure metamorphism (by the example of rocks of the Kokchetav massif). Russian Geology and Geophysics, 47(4), 482-496.

Sheldrick, G.M. (2008) A short history of SHELX. Acta Crystallographica, A64, 112–122.

Shieh, S.R., and Duffy, T.S. (2002) Raman spectroscopy of $Co(OH)_2$ at high pressures: Implications for amorphization and hydrogen repulsion. Physical Review B, 66, 134301-1–134301-8.

Sebastian, P.J., and Calixto, M.E. (2000) Porous CdS:CdO composite structure formed by screen printing and sintering of CdS in air. Thin Solid Films, 360 (1-2), 128–132.

Selby, D., and Creaser, R.A. (2003) Re–Os geochronology of organic rich sediments: an evaluation of organic matter analysis methods. Chemical Geology, 200, 225-240.

Smyth, J.R., Jacobsen, S.D., and Hazen, R.M. (2000) Comparative crystal chemistry of dense oxide minerals. *In:* High-temperature and high-pressure crystal chemistry. Reviews in Mineralogy and Geochemistry, 41, 157–186.

Sokol, E.V., Nigmatulina, E.N., and Volkova, N.I. (2002) Fluorine Mineralization from Burning Coal Spoil Heaps in the Russian Urals. Mineralogy and Petrology, 75, 23–40.

Sokol, E.V., Maksimova, N.V., Nigmatulina, E.N., Sharygin, V.V., and Kalugin, V.M. (2005) Combustion Metamorphism, 284p. Publishing House of the Siberian Branch of the Russian Academy of Science, Novosibirsk (in Russian).

Sokol, E.V., Gaskova, O.L., Kokh, S.N., Kozmenko, O.A., Seryotkin, Yu.V., Vapnik, Ye., and Murashko, M.N. (2011) Chromatite and its Cr^{3+}- and Cr^{6+}-bearing precursor minerals from the Nabi Musa Mottled Zone complex, Judean Desert. American Mineralogist, 96, 659-674.

Sokol, E.V., Kokh, S.N., Vapnik, Thiéry V., and Korzhova, S.A. (2014) Natural analogues of belite sulfoaluminate cement clinkers from Negev desert, Israel. American Mineralogist, 99, 1471-1487.

Sprung, S. (1985) Technological Problems in Pyroprocessing Cement Clinker: Cause and Solution, 1st ed. Beton-Verlag, Düsseldorf.

Srihari, V., Sridharan, V., Chandra, S., Sastry, V.S., Sahu, H.K., and Sundar, C.S. (2011) Wide band gap tunability of bulk $Cd_{1-x}Ca_xO$. Journal of Applied Physics, 109 (1), 013510-1–103510-7.

Taylor, H.F.W. (1997) Cement Chemistry, second edition, 459 p. Thomas Telford Services, London.

Techer, I., Khoury, H.N., Salameh, E., Rassineux, F., Claude, C., Clauer, N., Pagel, M., Lancelot, J., Hamelin, B., and Jacquot, E. (2006) Propagation of high-alkaline fluids in an argillaceous formation: Case study of the Khushaym Matruk natural analogue (Central Jordan). Journal of Geochemical Exploration, 90, 53–67.

Tilley, C.E. (1951) A note on the progressive metamorphism of siliceous limestones and dolomites. Geological Magazine, 88, 175–178.

Treiman, A.H., and Essene, E.J. (1983) Phase equilibria in the system CaO-SiO2-CO2. American Journal of Science, 283-A, 97–120.

Vaks, A., Bar-Matthews, M., Matthews, A., Ayalon, A., and Frumkin, A. (2010) Middle-Late Quaternary paleoclimate of northern margins of the Saharan-Arabian Desert: Reconstruction from speleothems of Negev Desert, Israel. Quaternary Science Reviews, 29, 2647–2662.

Yang, Yu., Xue, J., and Huang, Q. (2014) Studies on the solidification mechanisms of Ni and Cd in cement clinker during cement kiln co-processing of hazardous wastes. Construction and Building Materials, 57, 138–143.

Ye, L., Cook, N.J., Liu, T., Ciobanu, C.L., Gao, W., and Yang, Y. (2012) The Niujiaotang Cd-rich zinc deposit, Duyun, Guizhou province, southwest China: ore genesis and mechanisms of cadmium concentration. Miner Deposita, 47, 683–700.

Ye, L., and Liu, T. (1999) Sphalerite Chemistry, Niujiaotang Cd-Rich Zinc Deposit, Guizhou, Southwest China. Chaise Journal of Geochemistry, 18 (1), 62–68.

Yogeeswaran, G., Chenthamarakshan, C.R, Seshadri, A., de Tacconi, N.R., and Rajeshwar, K. (2006) Cathodic electrodeposition in the ternary Zn-Cd-O system: mixed $(ZnO)_x(CdO)_{1-x}$ film formation versus Cd-doping of ZnO films. Thin Solid Films, 515, 2464–2470

Zambonini, F. (1936) Mineralogia vesuviana. Quercigh, E (editor): 2nd edition. Atti della Reale Accademia delle Scienze Fisiche e Matematiche di Napoli. Rosenberg & Sellier Publishers, Torino/IT: pp436.

Zateeva, S.N., Sokol, E.V., and Sharygin, V.V. (2007) Specificity of pyrometamorphic minerals of the ellestadite group. Geology of Ore Deposits, 49, 8, 792–805.

Zhang, J. (1999) Room-temperature compressibilities of MnO and CdO: further examination of the role of cation type in bulk modulus systematics. Physics and Chemistry of Minerals, 26, 644–648.

Ziegler, M.A. (2001) Late Permian to Holocene paleofacies evolution of the Arabian plate and its hydrocarbon occurrences. GeoArabia, 6, 445–505.

Figure captions

FIGURE 1. Geological map of Daba-Siwaqa area in central Jordan, showing occurrences of combustion-metamorphic marbles. Modified after Khoury et al. (2015).

FIGURE 2. (a) Exposures of dark fresh marble enclosed in altered material of lighter color, (b) retrograde alteration along joints and brecciation in marbles of variable color; (c) hand specimen of gray-greenish layered spurrite-fluorellestadite marble enriched in lime-monteponite solid solution minerals (sample TH-72).

FIGURE 3. BSE images of bituminous phosphatic chalk (oil-shale) of the lower Muwaqqar Chalk Marl Formation.

(a) biomicritic matrix with Cd-rich wurtzite and framboidal pyrite;

(b) batch of diatom frustules and radiolaria spicules (opal-CT), with micrometer platy Cd-rich wurtzite crystallites;
(c) intergrowth of platy Cd-rich wurtzites;
(d) platy Cd-rich wurtzites clustered inside a chamber of *Turrilina* shell;
(e) foraminifera (*Subbotina* and *Turrilina*) chambers filled with S-rich bitumen;
(d) tetrahedral Cd-rich sphalerite in a chalk matrix and simple twinned pseudooctahedral sphalerite (inset).
Py = pyrite; *Sp* = sphalerite, *Wur* = wurtzite

FIGURE 4. BSE images of (Ca,Cd)O and associated minerals.
(a) a fragment of typical Zn- and Cd-rich spurrite-fluorellestadite marble with a nest of tululite and (Ca,Cd)O grains, sample DT-7;
(b) fluorapatite, brownmillerite and fluormayenite from a rock fragment leached by diluted HAc, sample TH-72;
(c, d) a typical assemblage of (Ca,Cd)O–bearing spurrite-fluorapatite marble: rock-forming calcite and fluorapatite, less abundant spurrite and brownmillerite, and accessory cuprite and (Ca,Cd)O. Note a (Ca,Cd)O grain rimmed by Cd-rich portlandite. Samples TH-18 and DT-7, respectively.
Mineral names are abbreviated as *Ap* = fluorapatite; *Brm* = brownmillerite, *Cal* = calcite, *Cpr* = cuprite, *Els* = fluorellestadite, *May* = fluormayenite; *Prt* = Cd-rich portlandite, *Spu* = spurrite, *Tul* = tululite.

FIGURE 5. Photomicrographs of (Ca,Cd)O and associated minerals and elemental (Zn, Al, Ca, Cd, Si, Mg, S, P) maps. Sample TH-72. Mineral name abbreviations: *Els* = fluorellestadite, *Cal* = calcite, *Per* = periclase, *Spu* = spurrite, *Tul* = tululite.

FIGURE 6. Photomicrographs of (Ca,Cd)O grains.
(a, c) (Ca,Cd)O anhedral inclusions in calcite and fluorellestadite. Photomicrograph in polarized transmitted and reflected light, respectively;
(b) a particle of (Ca,Cd)O, with cleavage along {111} (?) and inclusions of flourellestadite/fluorapatite and calcite, BSE image;
(d) (Ca,Cd)O grains rimmed by $CaCd(OH)_4$, BSE image;
(e) a (Ca,Cd)O particle faceted by imperfect {100} and {111} dominant forms, photomicrograph in polarized transmitted light;
(f) a fresh (Ca,Cd)O anhedral grain; BSE image.

(a, b, c, d, e) samples DT-7 and (f) sample TH-72. Mineral name abbreviations: *Ap* = fluorapatite, *Brm* = brownmillerite, *Cal* = calcite, *Els* = fluorellestadite, *Per* = periclase, *X-phase* = Ca_2UO_5•2-3H_2O

FIGURE 7. Compositional variations of (Ca,Cd)O solid solution series minerals in samples TH-18, TH-72, TH-74, and DT-7, (a) in weight percentages of CaO and CdO, and (b) in atoms per formula unit – apfu.

FIGURE 8. 2D frame from single-crystal X-ray diffraction of $(Ca_{0.49}Cd_{0.51})O$ in sample DT-7. Arrowed partial Debye fringes are attributed to $CaCd(OH)_4$ from alteration.

FIGURE 9. Raman spectra from sample DT-7, (a) on a single grain of $(Ca_{0.49}Cd_{0.51})O$, and (b) alteration rim of $CaCd(OH)_4$. Peak indexing according to Rieder et al. (1973).

FIGURE 10. Photomicrographs and elemental (Cd, Ca, F, Cl, O) maps of (Ca,Cd)O and secondary phases after (Ca,Cd)O. Sample TH-18. Mineral name abbreviations: *Brm* = brownmillerite, *Cal* = calcite, *Fl* = fluorite, *Prt* = Cd-rich portlandite, *Spu* = spurrite.

TABLE 1. Bulk whole-rock compositions in main oxides [wt%] and trace elements [ppm] by ICP-AES and SR XRF, of impure chalk-marl precursor (DOS-1), and combustion-metamorphic marbles (DT, TH) from the Tulul Al Hammam area, central Jordan.

Sample	LLD	DOS-1	DT-7	TH-74	TH-72	TH-18	TH-11
main oxides [wt%]							
SiO_2	0.25	19.3	3.67	3.40	4.00	4.40	4.85
TiO_2	0.10	0.16	*<0.10*	0.05	*<0.10*	*<0.10*	*<0.10*
Al_2O_3	0.25	2.64	0.46	1.05	1.10	1.20	1.17
Fe_2O_3-total	0.20	1.22	0.38	0.79	0.49	0.47	0.45
MgO	0.20	0.43	0.36	0.69	0.53	0.63	0.62
CaO	0.25	23.0	56.4	51.5	53.0	55.0	53.7
Na_2O	0.05	0.14	0.06	0.05	0.27	0.21	0.22
K_2O	0.05	0.29	*<0.05*	0.01	*<0.05*	*<0.05*	*<0.05*
P_2O_5	0.03	3.32	7.18	0.35	3.44	4.54	4.36
SO_3	0.05	9.83	0.38	*<0.05*	1.40	1.10	0.54
LOI	0.05	39.2	30.1	41.7	34.8	32.4	33.3
Total	–	99.5	99.0	99.5	99.0	100.0	99.2
trace elements [ppm]							
Ba	1.0	58.1	100	212	134	124	253
Cd	0.5	224	113	75	697	100	28
Cr	1.5	412	1100	36.3	579	1370	119
Cu	1.0	104	186	18.8	220	156	28.1
Mo	0.2	178	8.5	3.2	6.04	11.5	12.6
Ni	1.0	256	300	115	457	176	119
Pb	0.8	12.0	2.7	1.4	14.5	1.4	0.8
Sr	1.0	603	1600	967	1590	1340	968
Th	1.0	1.98	0.99	2.9	7.3	*<1.0*	4
U	1.0	36.6	54	6.2	24	27	9.1
V	2.0	338	300	52	457	340	130
Y	0.2	*n.a.*	73	113	36	41	25.8
Zn	1.0	1498	1300	333	1437	1430	470
Zr	0.5	34.2	100	20.7	67	19	21.2
Zn/Cd	–	6.69	11.50	4.44	2.06	14.30	16.67
Cd/Zn	–	0.150	0.087	0.225	0.485	0.070	0.060

Notes: n.a. = not analyzed; MnO < 0.01wt%, Co < 5 ppm.

TABLE 2**.** Mineral assemblages of combustion-metamorphic marbles from the Tulul Al Hammam area, central Jordan.

Sample/ Rock type	Main and *minor* phases	Accessory phases	Alteration products
DT-7 Spurrite-fluorapatite marble	Calcite, Fluorapatite ((SiO_4)-bearing), Spurrite, *Brownmillerite*	**(Ca,Cd)O**, **Tululite**, Periclase (Zn-, Cu-, Ni-rich), Chlormayenite, Cuprite, Tenorite	**$CaCd(OH)_4$**, CSHs after spurrite (sometimes Zn-bearing), Partially hydrated or hydroxylated Chlormayenite, Si-bearing hydrated $CaO-UO_3$ compounds
TH-72 Spurrite-fluorellestadite marble	Calcite, Fluorellestadite *Spurrite*, *Periclase (Zn, Ni, Co, Cu – rich)*	**(Ca,Cd)O**, **Zincite (Cd-bearing), Tululite**, Brownmillerite, Dorrite, $CaUO_4$, Ca_2UO_5, Ca_3UO_6, Lakargiite, Fluormayenite, Cassiterite, Cerianite, Fluorite, Halite	**$Cd(OH)_{2-x}Cl_x$,** CSHs (sometimes Zn- and U-bearing), Cl-bearing Hydrogarnets, Partially hydrated or hydroxylated Fluormayenite, Ca aluminate fluoride hydrated, Si-bearing hydrated $CaO-UO_3$ compounds, Brucite
TH-18 Spurrite-fluorellestadite marble	Calcite, Spurrite, Fluorellestadite	**(Ca,Cd)O**, Brownmillerite, Periclase (Zn, Cu, Ni-rich), Fluormayenite, Fluorite	**Cd-rich portlandite $(Ca,Cd)(OH)_2$**, Bultfonteinite ($Ca_2SiO_2(OH,F)_4$), CSHs (sometimes Zn-bearing), Ca aluminate fluoride hydrated, Si- and F-bearing hydrated $CaO-UO_3$ compounds, Brucite
TH-11 Fluorapatite marble	Calcite, Fluorapatite, Fluorellestadite	**(Ca,Cd)O**, Brownmillerite, Zinkite, Lakargiite, Bunsenite, Lime, Baryto-celestine, Galena, Sphalerite, Ag^0, Ag_2S, Iodargirite	CSHs Tyuyamunite or Metatyuyamunite, Chlorite (?) Zn- and Ni-bearing

Notes: main phases (> 10 vol %), minor phases (5-10 vol %) and *accessories* (< 3 vol %).
Cd-bearing minerals are in bold.

TABLE 3. Selected typical and calculated average compositions [wt%] of lime-monteponite solid-solution minerals in combustion-metamorphic marbles.

Sample	LLD	TH-72			average n=15	TH-18			average n=20	DT-7	*		average n=7
SiO_2	0.01	0.02	0.04	0.02	0.03	0.02	0.03	b.d.	0.02	n.a.	n.a.	n.a.	–
CaO	0.01	31.5	32.7	31.8	31.9	41.5	39.9	41.4	41.1	35.1	29.8	26.5	32.8
FeO	0.02	0.03	0.05	0.04	0.03	b.d.	b.d.	0.03	b.d.	n.a.	n.a.	n.a.	–
Al_2O_3	0.02	b.d.	b.d.	b.d.	b.d.	b.d.	0.03	b.d.	b.d.	n.a.	n.a.	n.a.	–
TiO_2	0.01	b.d.	0.02	0.02	b.d.	n.a.	n.a.	n.a.	n.a.	n.a.	n.a.	n.a.	–
ZnO	0.07	0.25	0.34	0.93	0.39	0.19	0.19	0.24	0.20	n.a.	n.a.	n.a.	–
CdO	0.07	67.8	66.0	66.8	67.1	58.5	59.9	58.6	59.5	64.5	69.7	73.3	66.4
Total	–	99.6	99.1	99.6	99.5	100.2	100.1	100.3	100.8	99.6	99.5	99.8	99.2
Formula based on one oxygen, in apfu													
Ca		0.51	0.53	0.52	0.52	0.62	0.60	0.62	0.61	0.55	0.49	0.45	0.53
Zn		0.00	0.00	0.01	0.00	0.00	0.00	0.00	0.00	–	–	–	–
Cd		0.48	0.47	0.47	0.48	0.38	0.39	0.38	0.39	0.45	0.51	0.55	0.47
Σ		1.00	1.00	1.00	1.00	1.00	1.00	1.00	1.00	1.00	1.00	1.00	1.00

Notes: b.d. = below detection; n.a. = not analyzed; n = number of analyses. SrO < 0.04, MgO < 0.02.
* the grain selected for X-ray single crystal structure determination.

TABLE 4. Data collection and structure refinement details for $(Ca_{0.49}Cd_{0.51})O$

Space group		$Fm\bar{3}m$
a (Å)		4.75377(14)
V (Å^3)		107.427(6)
Z		4
ρ (g/sm^3)		5.703
Crystal size (mm)		0.05 × 0.04 × 0.03
θ range for data collection		7.44 to 31.19
Index ranges		$-6 \leq h,k,l \leq 6$
No. of measured reflections		497
No. of unique reflections		19
No. of observed reflections ($I > 2\sigma(I)$)		19
No. of parameters refined		4
R_{int}		0.0601
R1, wR2 all data		0.0094, 0.0201
GooF		0.283
Residual electron density (e/Å^3)		0.386, –0.247
Atomic parameters		
M	*x, y, z*	0, 0, 0
	Occ.	$Ca_{0.50(3)}$ $Cd_{0.50(3)}$
	U_{eq}	0.0076(2)
O	*x, y, z*;	0.5, 0.5, 0.5
	U_{eq}	0.0072(14)

TABLE 5. Backscatter images and semi-quantitative analysis by SEM-EDS (SDD) of altered (Ca,Cd)O grains

BSE image

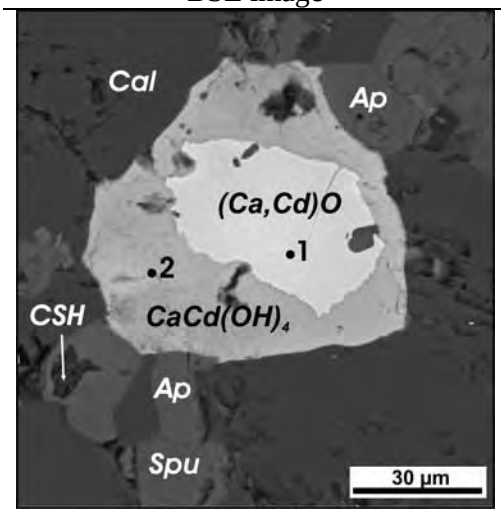

Chemical composition (wt %)

Sample DT-7

point	CaO	CdO	SiO_2	H_2O	F	Cl	O-$(F,Cl)_2$	Total
1 [a]	31.2	69.5	–	–	–	–	–	100.7
2 [b]	25.1	56.3	1.54	15.8[c]	–	0.4	0.09	99.2
$CaCd(OH)_4$ Ideal	25.4	58.2	–	16.3	–	–	–	99.9

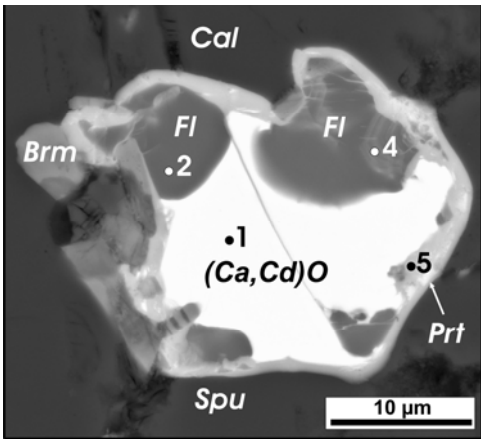

Sample TH-18

point	CaO	CdO	SiO_2	F	Cl	O-$(F,Cl)_2$	Total
1	40.2	60.5	–	–	–	–	100.7
2	68.5	2.46	–	47.6	0.27	20.0	98.8
4	63.0	10.5	0.62	42.8	0.69	18.2	99.4
5	34.4	43.6	0.64	1.79	0.28	0.82	79.9
CaF_2 ideal	71.8	–	–	48.7	–	20.5	100.0

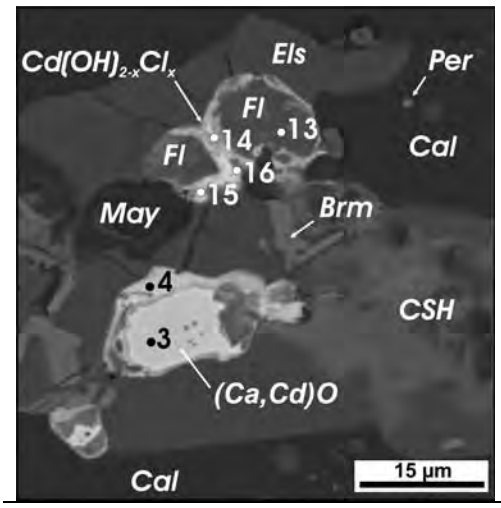

Sample TH-72

point	CaO	CdO	SiO_2	F	Cl	O-$(F,Cl)_2$	Total
3	32.3	68.7	–	–	–	–	101.0
4	14.7	66.0	0.68	1.91	11.3	3.35	91.2
13	68.9	1.40	–	47.9	0.48	20.3	98.4
14	11.9	71.4	–	8.72	8.86	5.67	95.2
15	16.3	56.0	0.98	–	9.87	2.23	80.9
16	11.3	70.8	–	5.37	10.2	4.56	93.1

Notes: Ap = fluorapatite; Brm = brownmillerite, Cal = calcite, CSH = calcium silicate hydrates, Els = fluorellestadite, Fl = fluorite, May = fluormayenite partially hydrated; Per = periclase, Prt = Cd-rich portlandite, Spu = spurrite, Tul = tululite. (a) mineral grain used for Raman spectrometry of (Ca,Cd)O; (b) mineral grain used for Raman spectroscopy of $CaCd(OH)_4$; (c) H_2O calculated from excess O contents.

TABLE 6. Partitioning of Cd and Zn among oxide minerals identified in combustion-metamorphic marble sample TH-72, Tulul Al Hammam, central Jordan.

Mineral	Space group	Cd in mineral, wt %	Cd in rock, wt %	K_{Cd}	Zn in mineral, wt %	Zn in rock, wt %	K_{Zn}	Substitution
Lime-monteponite ss (Ca,Cd)O	$Fm\bar{3}m$	58.8 (av.)	0.0697	843	0.75 (max.)	0.1437	≤5.2	$Ca^{[6]} \rightarrow Cd^{[6]}$
Tululite $(Ca,Cd)_{14}(Fe^{3+},Al)(Al,Zn,Fe^{3+},Si,P,Mn,Mg)_{15}O_{36})$	$F23$	7.48 (av.)	0.0697	107.3	17.4 (av.)	0.1437	121.4	$Ca^{[6]} \rightarrow Cd^{[6]}$
Zincite (Zn,Cd)O	$P6_3mc$	2.62 (max.)	0.0697	≤ 37.6	75.5 (av.)	0.1437	525.6	$Zn^{[4]} \rightarrow Cd^{[4]}$
Periclase (Mg,Zn,Ni,Cu)O	$Fm\bar{3}m$	< 0.02	0.0697	–	18.5 (av.)	0.1437	128.6	$Mg^{[6]} \rightarrow Zn^{[6]}$

Notes: $K_{Cd} = Cd_{mineral}/Cd_{rock}$; $K_{Zn} = Zn_{mineral}/Zn_{rock}$; av. = average, max. = maximal

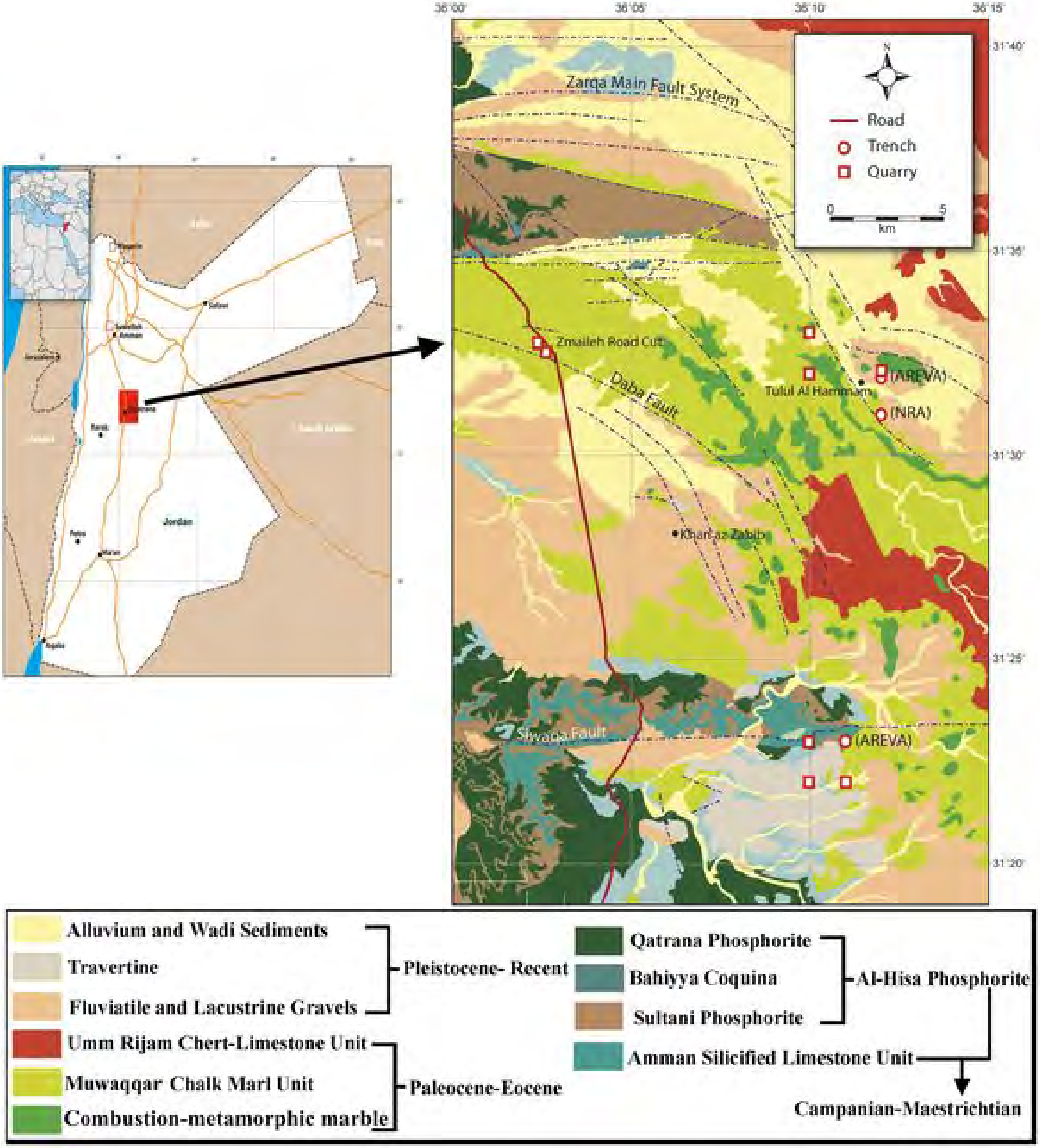
36°00'
36°05'
36°10'
36°15'
31°40'
31°35'
31°30'
31°25'
31°20'
Zarqa Main Fault System
Road
Trench
Quarry
0
5
km
Zmaileh Road Cut
Daba Fault
Tulul Al Hammam
(AREVA)
(NRA)
Khan az Zabib
Siwaqa Fault
(AREVA)
Jordan
Alluvium and Wadi Sediments
Travertine
Fluviatile and Lacustrine Gravels
Pleistocene- Recent
Umm Rijam Chert-Limestone Unit
Muwaqqar Chalk Marl Unit
Combustion-metamorphic marble
Paleocene-Eocene
Qatrana Phosphorite
Bahiyya Coquina
Sultani Phosphorite
Al-Hisa Phosphorite
Amman Silicified Limestone Unit
Campanian-Maestrichtian


A
B
C
2 cm

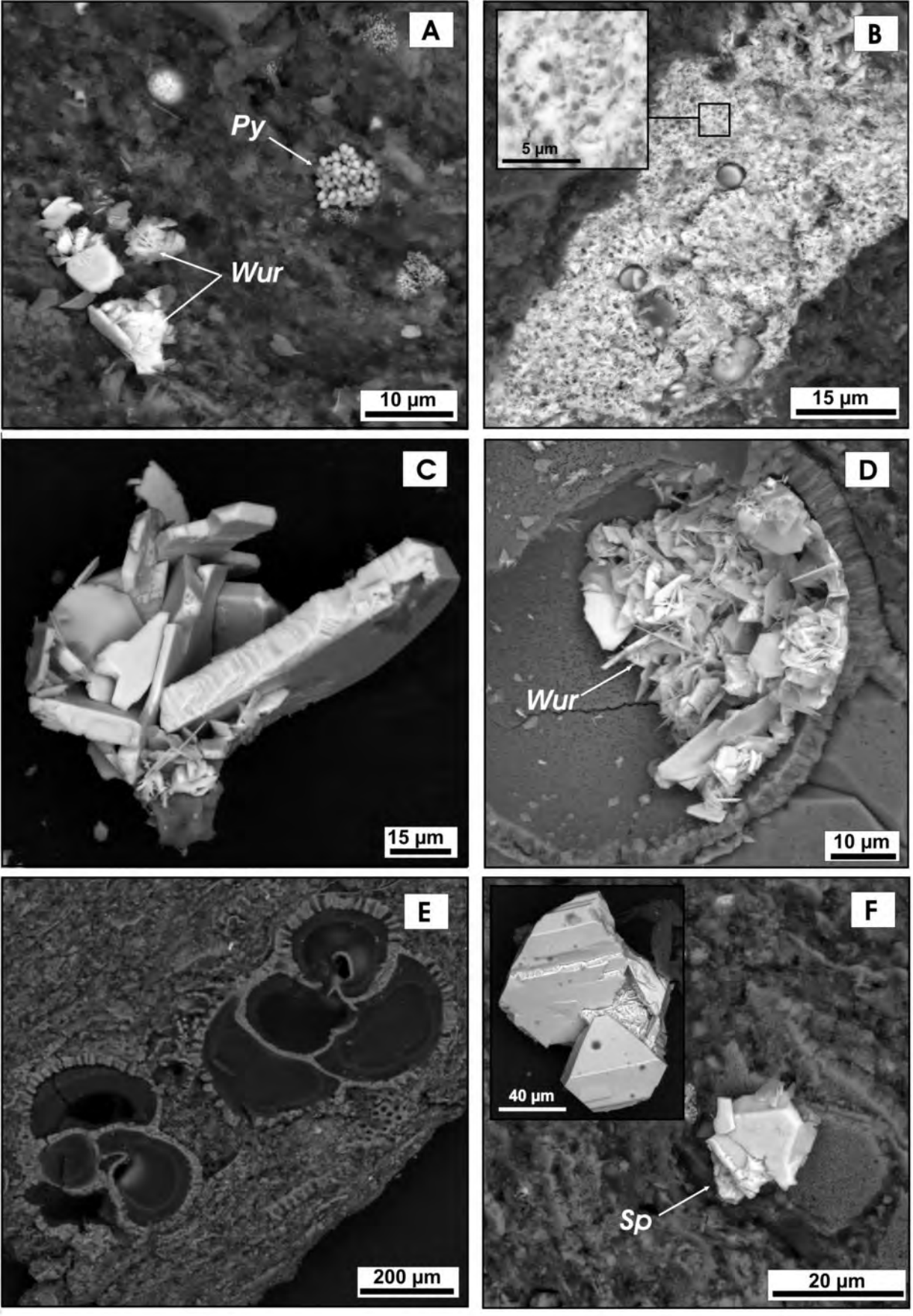
A
Py
Wur
10 µm
B
5 µm
15 µm
C
15 µm
D
Wur
10 µm
E
200 µm
F
40 µm
Sp
20 µm

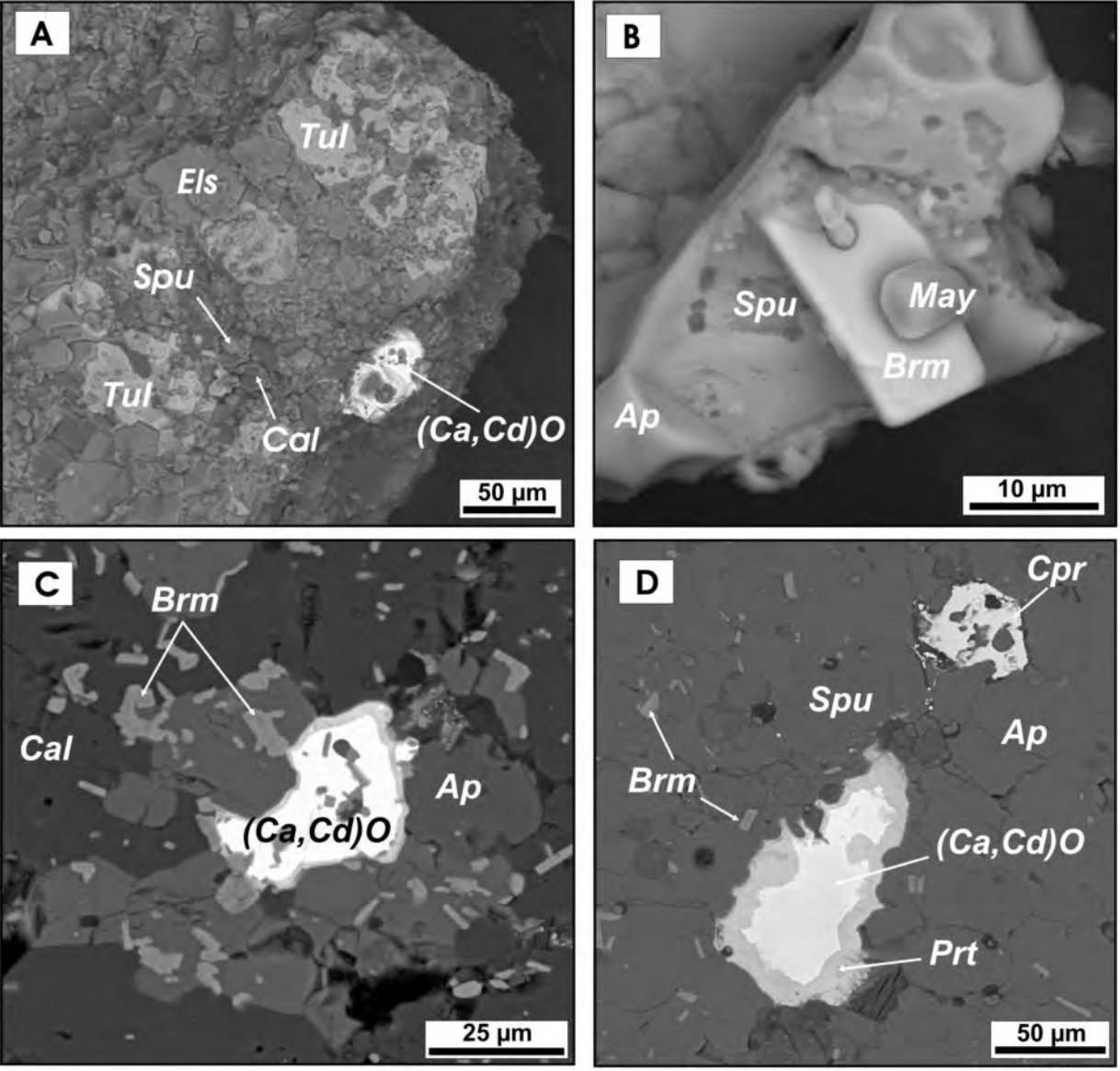
A
Tul
Els
Spu
Tul
Cal
(Ca,Cd)O
50 µm
B
Spu
May
Brm
Ap
10 µm
C
Brm
Cal
Ap
(Ca,Cd)O
25 µm
D
Cpr
Spu
Ap
Brm
(Ca,Cd)O
Prt
50 µm

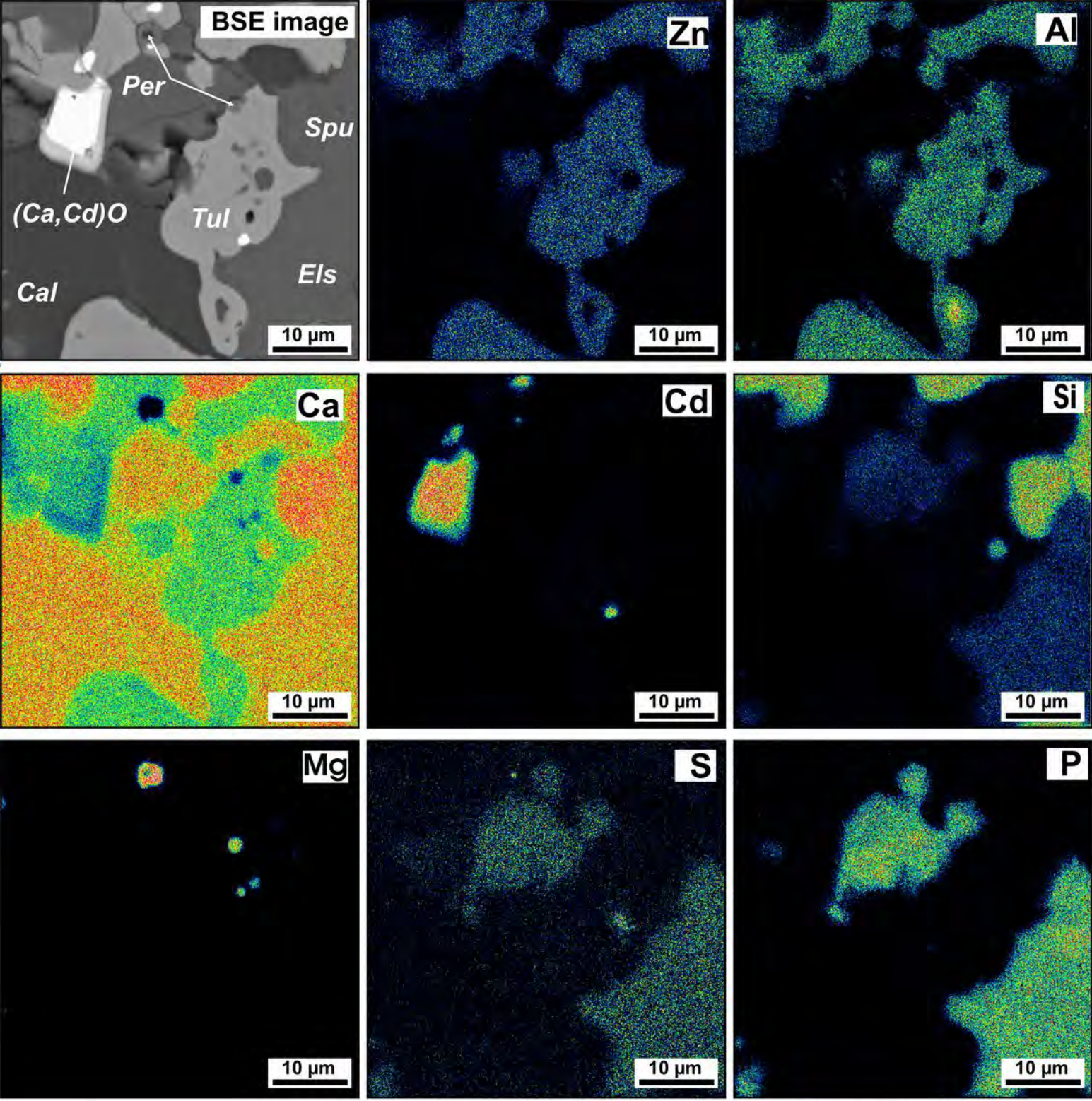
BSE image
Per
Spu
(Ca,Cd)O
Tul
Els
Cal
10 µm
Zn
10 µm
Al
10 µm
Ca
10 µm
Cd
10 µm
Si
10 µm
Mg
10 µm
S
10 µm
P
10 µm

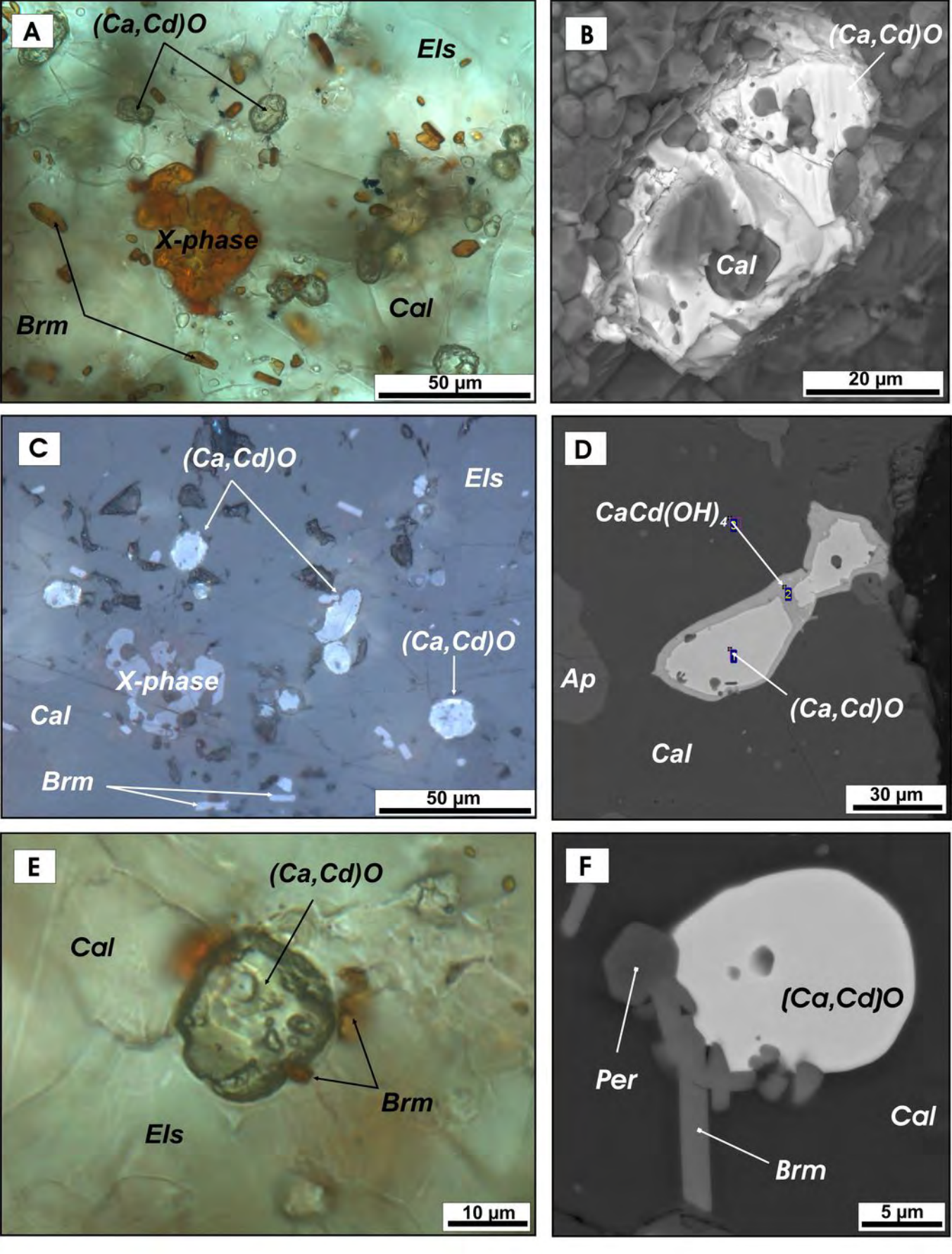
A
(Ca,Cd)O
Els
X-phase
Cal
Brm
50 µm
B
(Ca,Cd)O
Cal
20 µm
C
(Ca,Cd)O
Els
(Ca,Cd)O
X-phase
Cal
Brm
50 µm
D
CaCd(OH)4
Ap
(Ca,Cd)O
Cal
30 µm
E
(Ca,Cd)O
Cal
Brm
Els
10 µm
F
(Ca,Cd)O
Per
Cal
Brm
5 µm

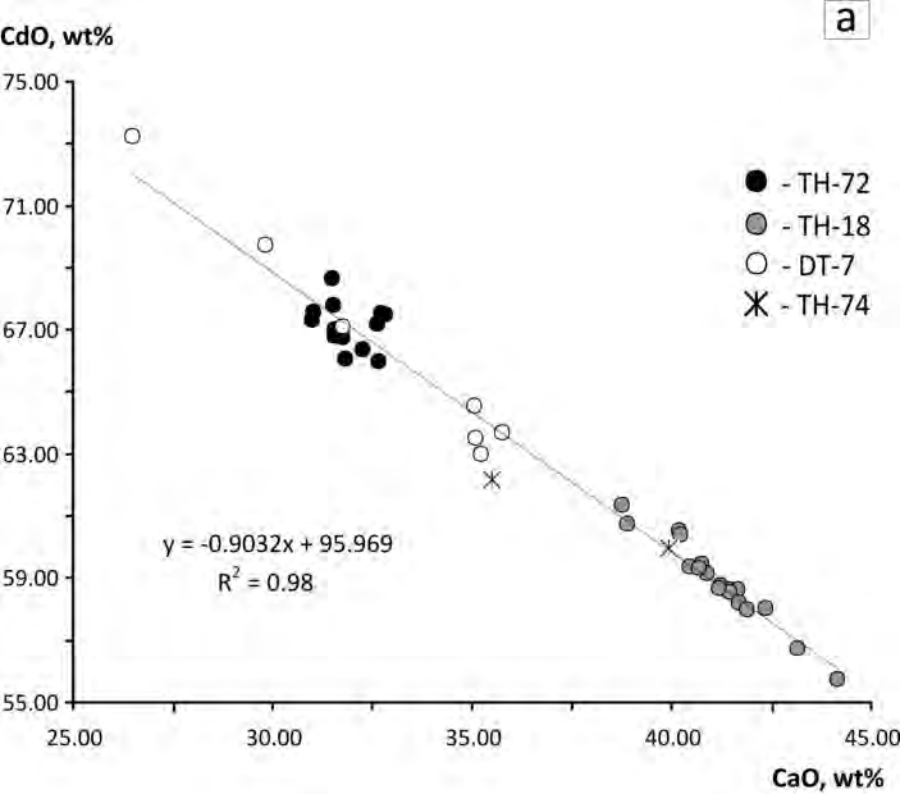
a
CdO, wt%
75.00
71.00
67.00
63.00
59.00
55.00
25.00
30.00
35.00
40.00
45.00
CaO, wt%
- TH-72
- TH-18
- DT-7
- TH-74
y = -0.9032x + 95.969
R2 = 0.98

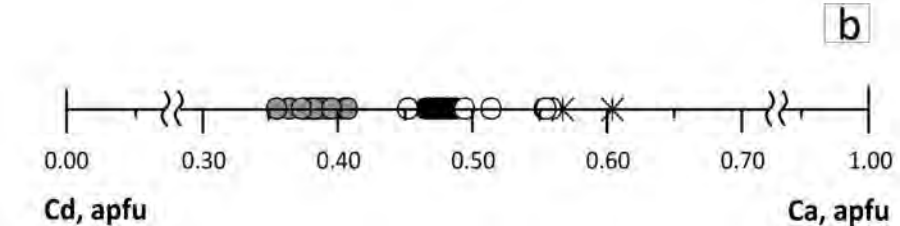
b
0.00
0.30
0.40
0.50
0.60
0.70
1.00
Cd, apfu
Ca, apfu

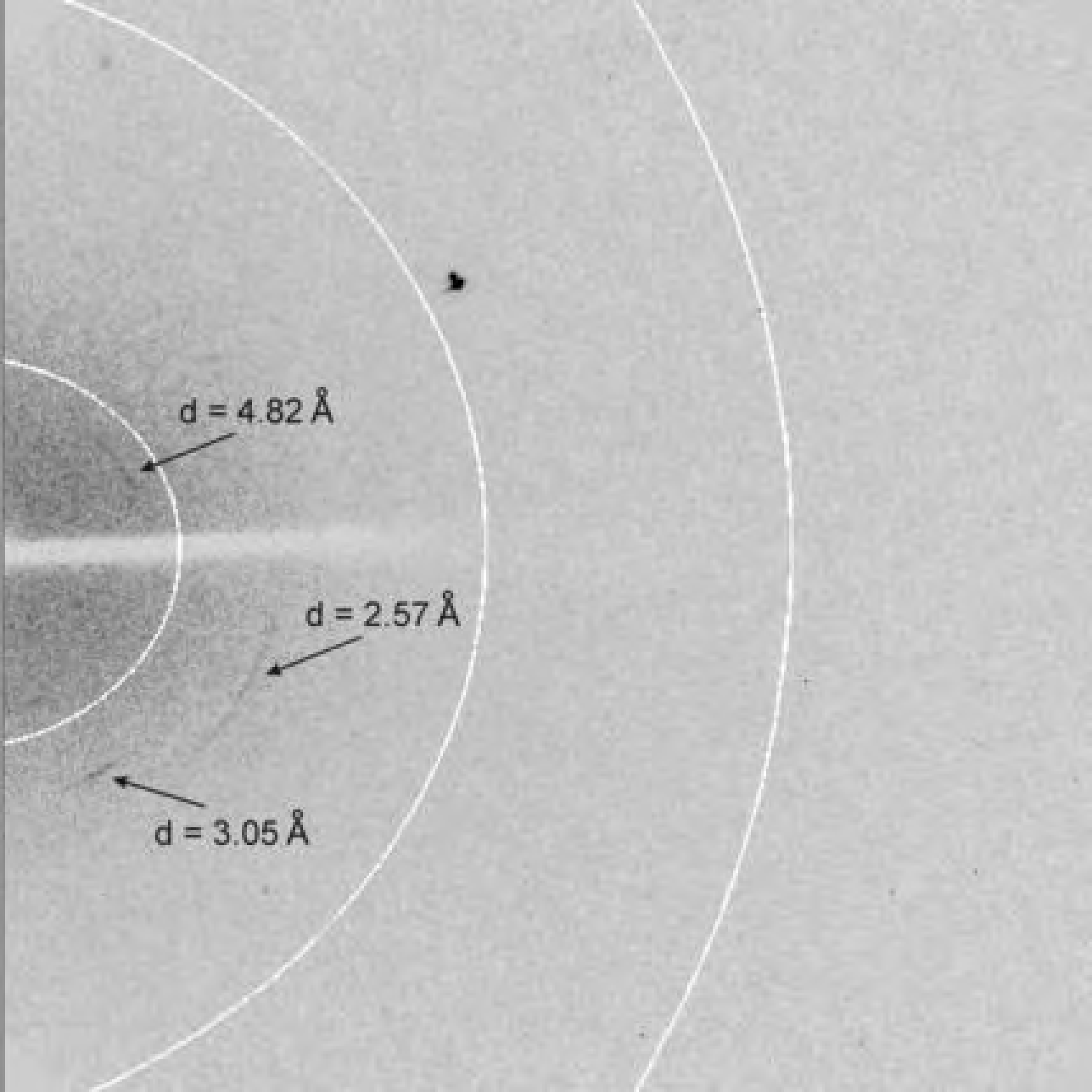
d = 4.82 Å
d = 2.57 Å
d = 3.05 Å

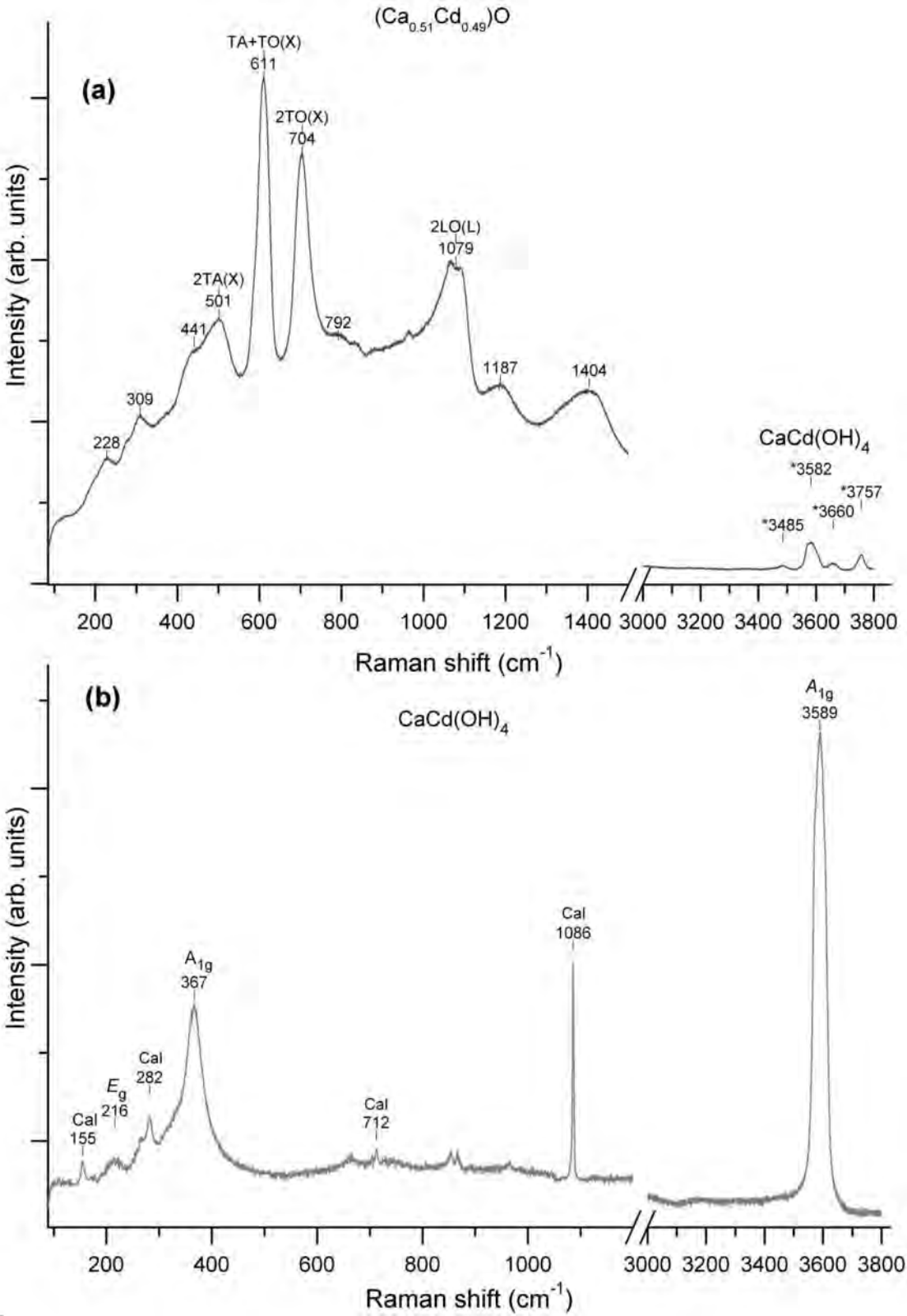
(Ca0.51Cd0.49)O
(a)
TA+TO(X)
611
2TO(X)
704
2LO(L)
1079
2TA(X)
501
441
792
1187
1404
309
228
CaCd(OH)4
*3582
*3757
*3660
*3485
Intensity (arb. units)
200
400
600
800
1000
1200
1400
3000
3200
3400
3600
3800
Raman shift (cm-1)
(b)
CaCd(OH)4
A1g
3589
Cal
1086
A1g
367
Cal
282
Eg
216
Cal
155
Cal
712
Intensity (arb. units)
200
400
600
800
1000
3000
3200
3400
3600
3800
Raman shift (cm-1)

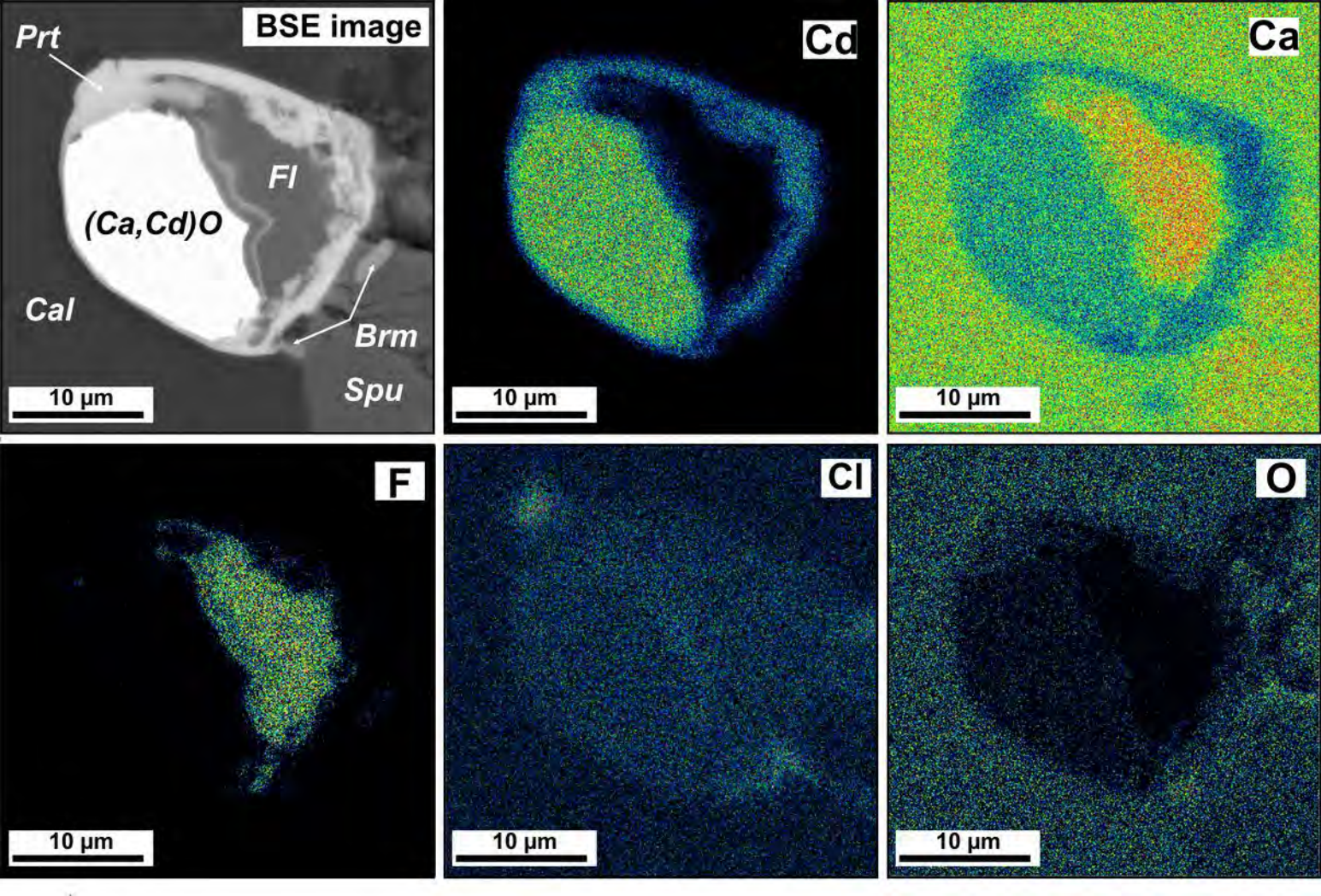
BSE image
Prt
Fl
(Ca,Cd)O
Cal
Brm
Spu
10 µm
Cd
10 µm
Ca
10 µm
F
10 µm
Cl
10 µm
O
10 µm